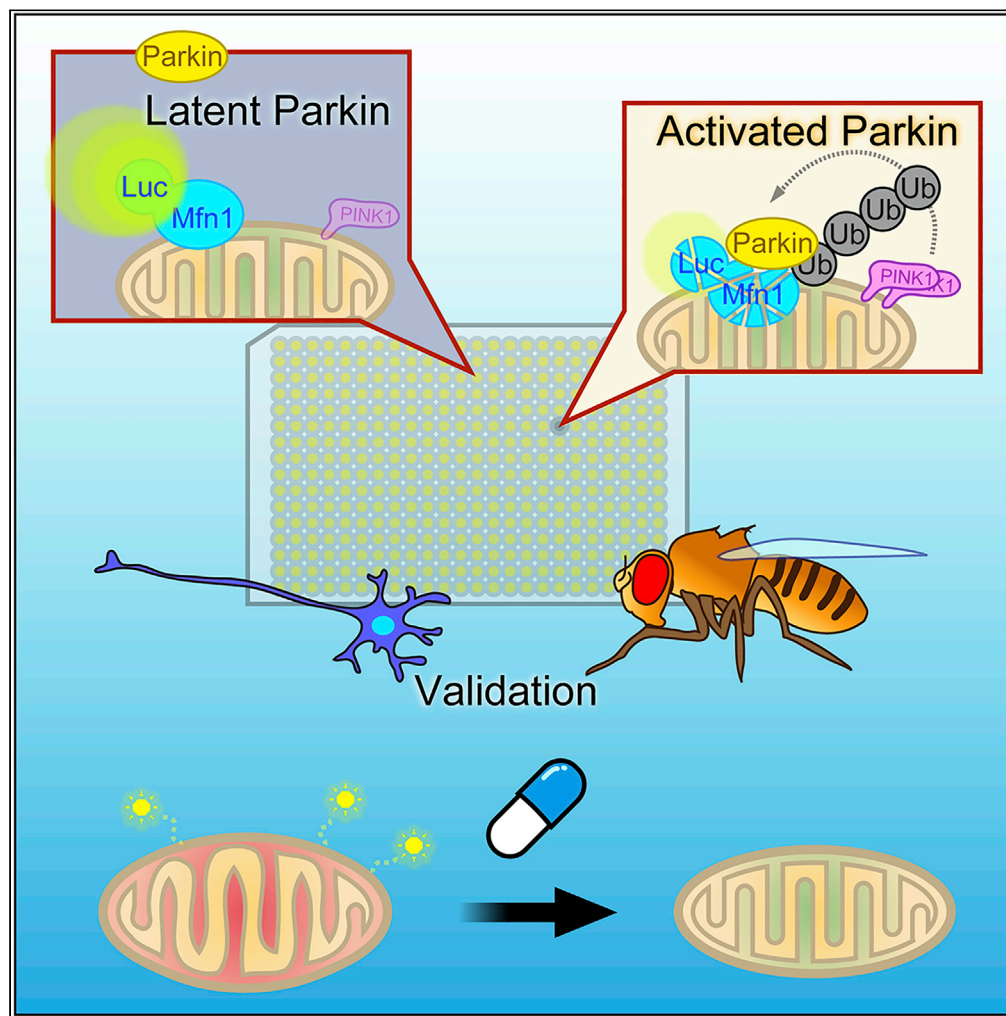# iScience

**Article**

# A Cell-Based High-Throughput Screening Identified Two Compounds that Enhance PINK1-Parkin Signaling



Kahori Shiba-Fukushima, Tsuyoshi Inoshita, Osamu Sano, ..., Wado Akamatsu, Yuzuru Imai, Nobutaka Hattori

yzimai@juntendo.ac.jp (Y.I.)
nhattori@juntendo.ac.jp (N.H.)

## HIGHLIGHTS

A high-throughput drug discovery system for PINK1-Parkin signaling was developed

The system identified two compounds that activate PINK1-Parkin signaling

Two compounds activated Parkin in human dopaminergic neurons and myoblasts

Two compounds improved mitochondrial functions of *PINK1*-knockdown *Drosophila*

CellPress
OPEN ACCESS

## Article

# A Cell-Based High-Throughput Screening Identified Two Compounds that Enhance PINK1-Parkin Signaling

Kahori Shiba-Fukushima,[1] Tsuyoshi Inoshita,[1] Osamu Sano,[2] Hidehisa Iwata,[2] Kei-ichi Ishikawa,[3,4] Hideyuki Okano,[5] Wado Akamatsu,[3] Yuzuru Imai,[4,6,7,*] and Nobutaka Hattori[1,4,6,*]

## SUMMARY

**Early-onset Parkinson's disease-associated PINK1-Parkin signaling maintains mitochondrial health. Therapeutic approaches for enhancing PINK1-Parkin signaling present a potential strategy for treating various diseases caused by mitochondrial dysfunction. We report two chemical enhancers of PINK1-Parkin signaling, identified using a robust cell-based high-throughput screening system. These small molecules, T0466 and T0467, activate Parkin mitochondrial translocation in dopaminergic neurons and myoblasts at low doses that do not induce mitochondrial accumulation of PINK1. Moreover, both compounds reduce unfolded mitochondrial protein levels, presumably through enhanced PINK1-Parkin signaling. These molecules also mitigate the locomotion defect, reduced ATP production, and disturbed mitochondrial $Ca^{2+}$ response in the muscles along with the mitochondrial aggregation in dopaminergic neurons through reduced PINK1 activity in *Drosophila*. Our results suggested that T0466 and T0467 may hold promise as therapeutic reagents in Parkinson's disease and related disorders.**

## INTRODUCTION

Homozygous or compound heterozygous mutations of genes encoding PINK1 and Parkin lead to the selective degeneration of midbrain dopaminergic neurons and cause autosomal recessive early-onset Parkinson's disease (PD) (Kitada et al., 1998; Valente et al., 2004). *Drosophila* and mammalian cell studies revealed that PINK1 and Parkin have roles in mitochondrial quality control (Clark et al., 2006; Matsuda et al., 2010; Narendra et al., 2010; Park et al., 2006; Yang et al., 2006). Subsequent studies using animal models for accelerated mitochondrial genomic error accumulation (Pickrell et al., 2015) and for mitochondrial stress through unfolded proteins (Pimenta de Castro et al., 2012) support the notion that PINK1 and Parkin maintain dopaminergic neuron survival through correcting the dysfunctional mitochondrial pool.

The PINK1 mitochondrial serine/threonine protein kinase is constitutively degraded by a combination of mitochondrial proteases and the ubiquitin-proteasome pathway in a mitochondrial membrane potential ($\Delta\Psi$m)-dependent manner (Jin et al., 2010). $\Delta\Psi$m reduction due to mitochondrial damage leads to PINK1 accumulation and activation at the outer mitochondrial membrane, preventing the $\Delta\Psi$m-dependent import of PINK1 to the internal mitochondrial compartment (Jin et al., 2010; Okatsu et al., 2015). Activated PINK1 phosphorylates the Parkin ubiquitin ligase (E3) and Ubiquitin (Kane et al., 2014; Kondapalli et al., 2012; Koyano et al., 2014; Ordureau et al., 2014; Shiba-Fukushima et al., 2012, 2014). Latent Parkin, in the cytosol, is activated and relocalized to the outer mitochondrial membrane, ubiquitinating mitochondrial proteins such as Mitofusin and Miro (Liu et al., 2012; Tanaka et al., 2010; Wang et al., 2011). Mitochondrial protein ubiquitination promotes mitochondrial recruitment of autophagy regulators and receptors such as TBK1 and optineurin (Heo et al., 2015; Matsumoto et al., 2015; Richter et al., 2016). The ubiquitination and subsequent degradation of Mitofusin and Miro promotes mitochondrial fragmentation and suppresses mitochondrial motility, respectively, and facilitates the autophagic removal of damaged mitochondria (Deng et al., 2008; Liu et al., 2012; Wang et al., 2011; Yang et al., 2008; Ziviani et al., 2010).

We developed a cell-based high-throughput screening (HTS) system to identify compounds (cpds) that could activate PINK1-Parkin signaling. Two unique cpds, T0466 (also known as compound 1) and T0467, were identified and characterized (Hildebrand et al., 2014). Both cpds successfully induced Parkin

[1]Department of Treatment and Research in Multiple Sclerosis and Neuro-intractable Disease, Juntendo University Graduate School of Medicine, Tokyo 113-8421, Japan

[2]BioMolecular Research Laboratories, Takeda Pharmaceutical Company, Fujisawa, Kanagawa 251-8555, Japan

[3]Center for Genomic and Regenerative Medicine, Juntendo University Graduate School of Medicine, Tokyo 113-8421, Japan

[4]Department of Neurology, Juntendo University Graduate School of Medicine, 2-1-1 Hongo, Bunkyo-ku, Tokyo 113-8421, Japan

[5]Department of Physiology, Keio University School of Medicine, Tokyo 160-8582, Japan

[6]Department of Research for Parkinson's Disease, Juntendo University Graduate School of Medicine, 2-1-1 Hongo, Bunkyo-ku, Tokyo 113-8421, Japan

[7]Lead Contact

*Correspondence: yzimai@juntendo.ac.jp (Y.I.), nhattori@juntendo.ac.jp (N.H.)

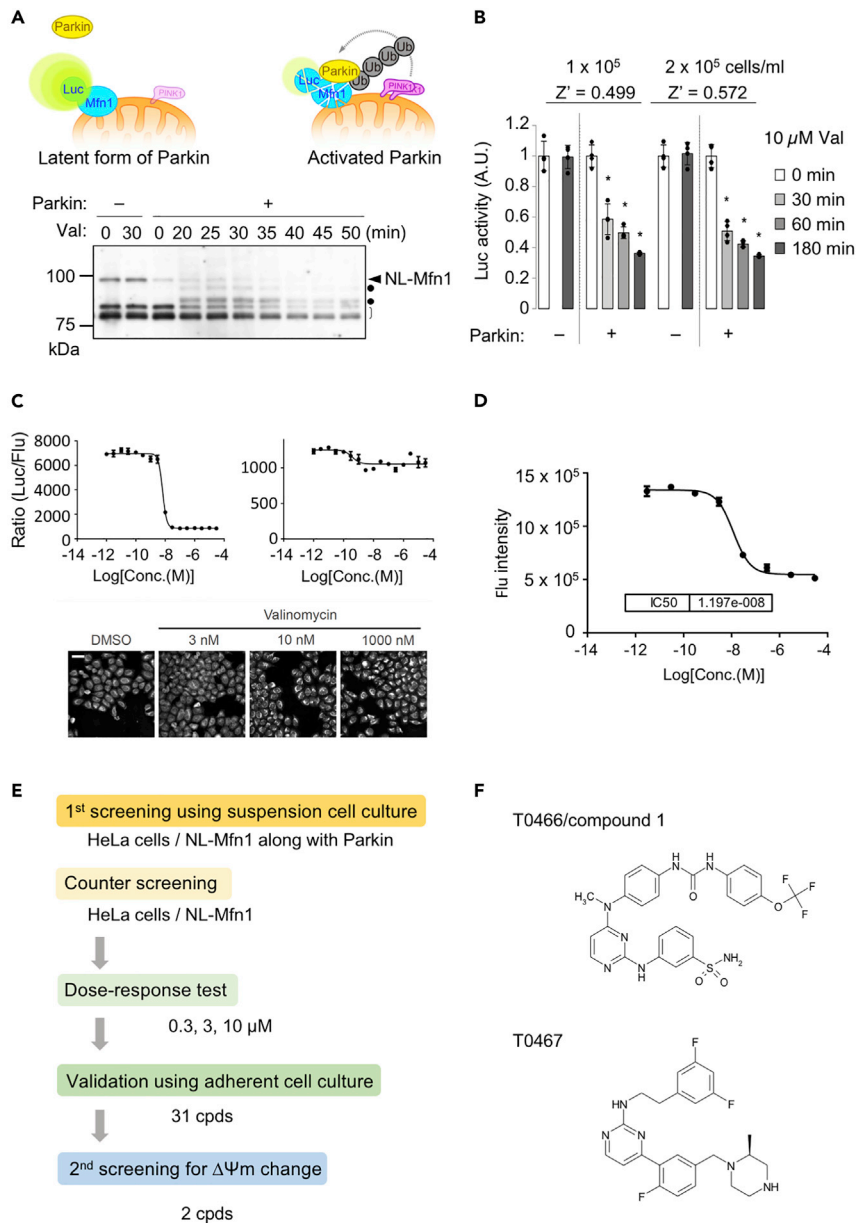https://doi.org/10.1016/j.isci.2020.101048

**Figure 1. Development of the NL-Mfn1 Screening System**

(A) (Top) Schema of the NL-Mfn1 reporter assay to monitor Parkin activity. (Bottom) Time course analysis of NL-Mfn1 degradation after PINK1 activation by valinomycin (Val) treatment. Lysate of HeLa cells expressing NL-Mfn1 in the presence or absence of Parkin treated with 10 μM Val were analyzed by western blot with anti-Mfn1. NL-Mfn1 (arrowhead), endogenous Mfn1 (open bracket) and ubiquitinated Mfn1 (dots) are shown.

(B) Validation of the NL-Mfn1 reporter assay using Val. NL activity was normalized using fluorescence signals monitoring cell viability and density in 96-well plates. The value of non-treatment (0 min) for each cell line was set as 1. Z′-factors for the given cell densities are also shown. Data are presented as mean $\pm$ SEM from four independent samples. *$p < 0.01$ by one-way ANOVA with Tukey-Kramer test.

(C) Val dose response in the NL-Mfn1 reporter assay. (Top) Graphs (mean $\pm$ SD, n = 2 independent samples) representing NL activity normalized using the fluorescence signals of HeLa cells expressing NL-Mfn1 in the presence (left) or absence (right) of Parkin and treated with the indicated doses of Val. (Bottom) PINK1 accumulation in reporter cells with Parkin under the same conditions. Scale bar, 50 μm.

(D) $\Delta\Psi$m assay validation using MitoTracker Red. Cells were treated as in (C). The IC$_{50}$ was $1.197 \times 10^{-8}$ M, at which the NL-Mfn1 reporter fully detected Parkin activation (see graphs in [C]). Data are presented as mean $\pm$ SD from eight independent samples.

**Figure 1. Continued**

(E) Screening flow. See Methods for details.

(F) Chemical structure of T0466 and T0467.

See also Figure S1.

mitochondrial translocation in dopaminergic neurons differentiated from iPS cells (iPSCs) without obvious $\Delta\Psi$m reduction and cell toxicity and eliminated unfolded mitochondrial protein caused by a truncation of ornithine carbamoyltransferase ($\Delta$OTC) from mitochondrial pools. In the *Drosophila PINK1* model, both cpds improved the motor defects, aggregated mitochondrial morphology and decreased ATP production caused by reduced PINK1 activity. Moreover, T0467 suppressed the altered mitochondrial $Ca^{2+}$ response caused by reduced PINK1 expression. These cpds may be promising drug candidates for diseases associated with mitochondrial damage.

## RESULTS

### Development of a Cell-Based HTS System for PINK1-Parkin Activation Drugs

Mitofusin family member, Mitofusin 1 (Mfn1), is rapidly degraded by active Parkin in association with mitochondrial depolarization-dependent PINK1 activation (Shiba-Fukushima et al., 2012). We developed a cell-based reporter system, described herein, that utilizes NanoLuc (England et al., 2016). Mfn1 was N-terminally fused with a newly developed luciferase, NanoLuc (NL), and this reporter was named NL-Mfn1. We generated HeLa cells stably expressing NL-Mfn1 with or without Parkin. NL-Mfn1 and endogenous Mfn1 were rapidly degraded in the presence of Parkin after mitochondrial depolarization by valinomycin (val) (Figure 1A). We isolated single cell clones expressing NL-Mfn1 to ensure robustness for large-scale drug screening. We evaluated the sensitivity of the NL-Mfn1 screening system using val, a PINK1-Parkin signaling activator. NL activity was sequentially measured to assess Mfn1 expression levels, and fluorescence signals were used to monitor cell density (see detail in Materials and Methods). The NL-Mfn1 screening system reliably detected Mfn1 degradation only in the presence of Parkin. This was observed by reduced NL activity in cells grown at two different densities, with a Z'-factor value of 0.50–0.57 (Figure 1B). The sensitivity of the NL-Mfn1 screening system was assessed using a series of val dilutions. The NL reporter responded in the presence of Parkin following treatment with over 10 nM of val. Under these conditions, PINK1 accumulation and $\Delta\Psi$m reduction were observed (Figures 1C and 1D). The NL-Mfn1 system also worked using cell suspensions, the sensitivity of which was comparable with that measured using adherent cells (Figure S1).

We applied the NL-Mfn1 system to a 1,536-well plate format and performed meso-scale drug discovery using the Takeda compound library (Figure 1E). Thirty-one candidates were assessed for $\Delta\Psi$m independence using the $\Delta\Psi$m assay. Two cpds, T0466 and T0467, were obtained as drug candidates for PINK1-Parkin signaling activation (Figures 1E and 1F).

### T0466 and T0467 Stimulate the Mitochondrial Translocation of Parkin in a PINK1-Dependent Manner

We tested whether T0466 and T0467 activate Parkin mitochondrial translocation. HeLa cells stably expressing GFP-Parkin (HeLa/GFP-Parkin cells) were treated with T0466 and T0467 at different concentrations. Over 5 μM of T0466 sufficiently stimulated the mitochondrial translocation of GFP-Parkin 3–8 h after treatment, whereas over 12 μM of T0467 was required for Parkin translocation (Figures 2A, S2A, and S2B). When HeLa/GFP-Parkin cells were treated with 5 μM T0466 or 20 μM T0467 for 3 h, GTP-Parkin was translocated to the mitochondria in approximately 44% and 21% of cells, respectively (Figure 2B). However, Parkin translocation by T0466 or T0467 did not occur when the E3-dead form of Parkin was expressed in place of wild-type Parkin, or in the absence of PINK1 activity, suggesting that PINK1 and Parkin activities are required for this effect (Figure 2C). Simultaneous treatment with a previously characterized PINK1 activation molecule, kinetin triphosphate (KTP), did not enhance T0466 or T0467 efficacy (Figure S2A) (Hertz et al., 2013).

Parkin activation relieves mitochondrial unfolded protein stress presumably through the mitophagic removal of mitochondria with accumulated unfolded proteins (Jin and Youle, 2013). $\Delta$OTC expression results in Triton X-100 insoluble protein aggregates in the mitochondrial matrix, leading to PINK1 activation and subsequent Parkin-mediated mitophagy without $\Delta\Psi$m reduction (Jin and Youle, 2013). We estimated the effects of T0466 or T0467 in this context. The mitochondrial inner membrane protein, OPA1, is
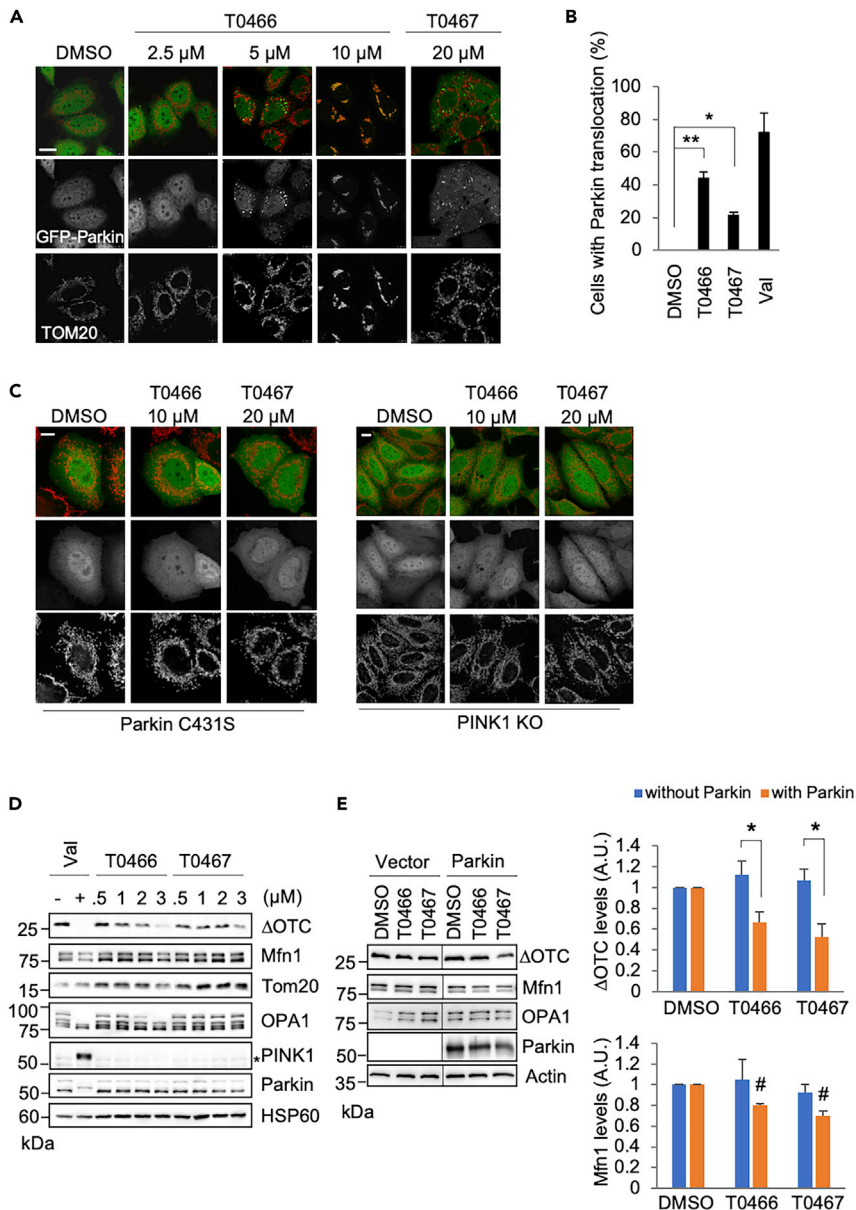
**Figure 2. T0466 and T0467 Activate Parkin, Which Reduces an Unfolded Mitochondrial Protein**

(A) T0466 and T0467 stimulate mitochondrial translocation of Parkin in HeLa cells. HeLa/GFP-Parkin cells were treated with the cpds at the indicated concentrations for 3 h. DMSO treatment served as a mock control. Mitochondria were visualized with anti-TOM20 staining. Scale bar, 20 μm.

(B) Mitochondrial translocation efficiency of Parkin by the cpds. HeLa/GFP-Parkin cells were treated with 5 μM T0466 and 20 μM T0467 for 3 h. The graph (mean ± SEM, n = 3 biological replicates) represents the percentage of cells with GFP-Parkin colocalized with TOM20. Cells treated with a mitochondrial uncoupling reagent Val (10 μM) served as the positive control. *$p < 0.005$, **$p < 0.0001$ versus DMSO using Dunnett's test.

(C) Parkin mitochondrial translocation by T0466 and T0467 is Parkin E3 activity- and PINK1-dependent. HeLa cells transfected with an E3 dead form of GFP-Parkin C431S (left) and *PINK1*-deficient HeLa cells (right, PINK1 KO) were treated with T0466 or T0467 as in (A). Scale bars, 25 μm.

(D) Unfolded mitochondrial protein (ΔOTC) is reduced by T0466 and T0467. ΔOTC/HeLa-TetOn cells with the stable expression of YFP-Parkin were treated with doxycycline (DOX, 1 μg/mL) for 72 h to induce mitochondrial ΔOTC expression. After removal of DOX, cells were treated with the indicated concentration of drugs for 8 h. Asterisk, non-specific.

(E) T0466 and T0467 promote ΔOTC degradation in the presence of Parkin. ΔOTC/HeLa-TetOn cells transfected with a mock vector or Parkin were treated with DOX (1 μg/mL) for 24 h. After removal of DOX, cells were treated with 2 μM T0466

**Figure 2. *Continued***
or 3 μM T0467 for 8 h. The relative band intensities of ΔOTC in 0.5% Triton X-100-insoluble fraction normalized with actin and of Mfn1 normalized with tubulin in 0.5% Triton X-100-soluble fraction are represented here (mean ± SEM, n = 4 biological replicates). *p < 0.05 by two-tailed Student's t test; #p < 0.01 versus DMSO with Parkin using Dunnett's test.
See also Figures S2 and S3.

processed at multiple sites in a ΔΨm reduction-dependent manner. OPA1 western blots can be used to monitor subtle ΔΨm changes (Ishihara et al., 2006). Monitoring of OPA1 processing revealed that higher T0466 concentrations reduced ΔΨm. However, a dose-dependent ΔOTC decrease was observed at T0466 concentrations as low as 1 μM, at which OPA1 was not processed in HeLa cells (Figure 2D). Moreover, T0467 induced the removal of ΔOTC without OPA1 processing, suggesting that these cpds facilitate Parkin activation independently of ΔΨm status. Consistent with these observations, these cpds did not elevate PINK1 levels, indicating that the molecular targets of these cpds are likely to be a protein other than PINK1. Using the cpds at concentrations that barely affected ΔΨm in HeLa cells (i.e., 2 μM for T0466 and 3 μM for T0467), we confirmed the Parkin dependence of ΔOTC degradation (Figure 2E). Mild degradation of Mn1 was also observed in the presence of Parkin. We next investigated the possibility that these two cpds directly activate Parkin. However, these cpds failed to stimulate Parkin E3 activity *in vitro* (data not shown), and there was no evidence that the cpds directly bind to Parkin (Figure S2C).

Previous studies have shown that T0466 has type II kinase inhibitor properties and could potentially target Ser/Thr and Tyr protein family kinases, including the MLKL pseudokinase (Hildebrand et al., 2014; Ma et al., 2016). Type II kinase inhibitors occupy the adenosine pocket of kinase domains, inducing a configuration change of the key residues required for kinase activity (Dar and Shokat, 2011). We tested the possibility that MLKL negatively regulates PINK1-Parkin signaling by monitoring the mitochondrial relocation of MLKL during PINK1-Parkin activation. GFP-MLKL was localized in the cytosol with occasional punctate signals. The subcellular localization of GFP-MLKL was not altered by T0466 or by mitochondrial uncoupling treatment (Figure S3A). Moreover, MLKL overexpression did not affect the mitophagy time course, suggesting that MLKL is unlikely to be a T0466 target in PINK1-Parkin signaling (Figure S3B).

We tested whether T0466 affects the activity of known kinases involved in PINK1-Parkin signaling, including PINK1 (Kondapalli et al., 2012; Shiba-Fukushima et al., 2012), TBK1 (Heo et al., 2015), and protein kinase A (PKA) (Akabane et al., 2016). *In vitro* kinase assays indicated that T0466 neither activated nor inhibited PINK1 kinase activity in the presence or absence of ATP (Figure S3C). T0466 treatment did not affect TBK1 activation in HeLa cells (Figure S3D). PKA negatively regulates PINK1 levels through MIC60 phosphorylation (Akabane et al., 2016). *In vitro* kinase assays showed that T0466 does not affect MIC60 phosphorylation by PKA (Figure S3E). These results suggest that T0466 does not modulate PINK1, TBK1, and PKA kinase activities.

## T0466 and T0467 Activate Parkin in Dopaminergic Neurons

We examined the effects of T0466 and T0467 on dopaminergic neurons, which are degenerated during the development and progression of PD. We first tested the effects of T0466 and T0467 on cell toxicity and mitochondrial functions. Treatments with T0466 and T0467 at concentrations of 0.1–1 μM did not show any cell toxicity by 48 h (Figure S4A). ATP production was moderately stimulated by lower concentrations (0.1–0.6 μM) of both cpds at 24 h, whereas treatment with 1 μM T0466 mildly reduced ATP production at 24 and 48 h (Figure S4B). We evaluated the effects of the cpds on ΔΨm in dopaminergic neuron cultures at higher concentrations. Treatment with more than 3 μM of T0466 for 8 h caused a small increase in OPA1 processing and low levels of PINK1 accumulation (Figure 3A, lanes 4 and 5), whereas 5 μM T0467 did not affect OPA1 processing and PINK1 levels (Figure 3A, lane 8). ATP production was compromised by ≥ 2.5 μM T0466 without acute cytotoxicity (Figures S4C and S4D). These results indicated that T0466 and T0467, at ≤1 μM and ≤2.5 μM, respectively, do not appear to be associated with occasional PINK1 activation by ΔΨm reduction and are appropriate for dopaminergic neuron cultures.

Parkin activation was monitored by its mitochondrial translocation. GFP-Parkin relocation from the whole cytosol to the punctate structures in dopaminergic neuron cultures was observed after treatment with 1 μM T0466 or 2.5 μM T0467 for 8 h, and the Parkin foci were overlapped with TOM20 signals, suggesting that Parkin activated by the drug treatment was translocated to the mitochondria (Figures 3B and 3C).
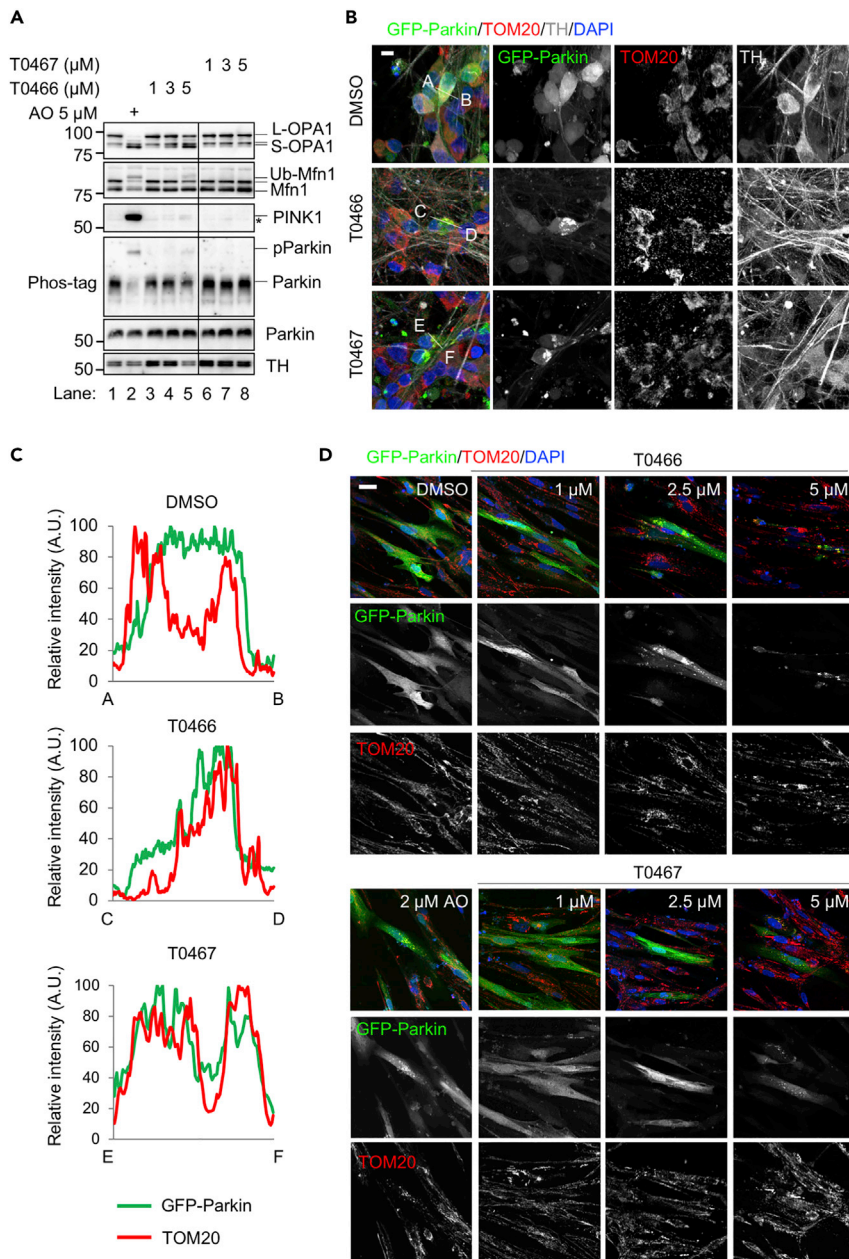
**Figure 3. T0466 and T0467 Activate Parkin in Human Dopaminergic Neurons and Myoblasts**

(A) Effects of T0466 and T0467 on the ΔΨm of dopaminergic neurons. Dopaminergic neurons differentiated from human iPSCs were treated with T0466 and T0467 at the indicated concentration for 8 h. Antimycin A and oligomycin (AO) were used as mitochondrial uncoupling reagents. Asterisk, non-specific.

(B and C) T0466 and T0467 stimulate Parkin mitochondrial translocation in dopaminergic neurons. (B) Dopaminergic neurons, with virally introduced GFP-Parkin (green), were treated with 1 μM T0466 or 2.5 μM T0467 for 8 h. Single channel images for GFP-Parkin and TOM20 are also shown (grayscale). Scale bar, 10 μm. (C) Line profiles of fluorescence intensity along cross-sections in the images shown in (B). A.U., arbitrary units.

(D) Myotubes forming from skeletal myoblasts, with virally introduced GFP-Parkin (green), were treated with the compounds at the indicated concentrations for 8 h. Mitochondria were visualized using anti-TOM20 staining (red). Scale bar, 25 μm.
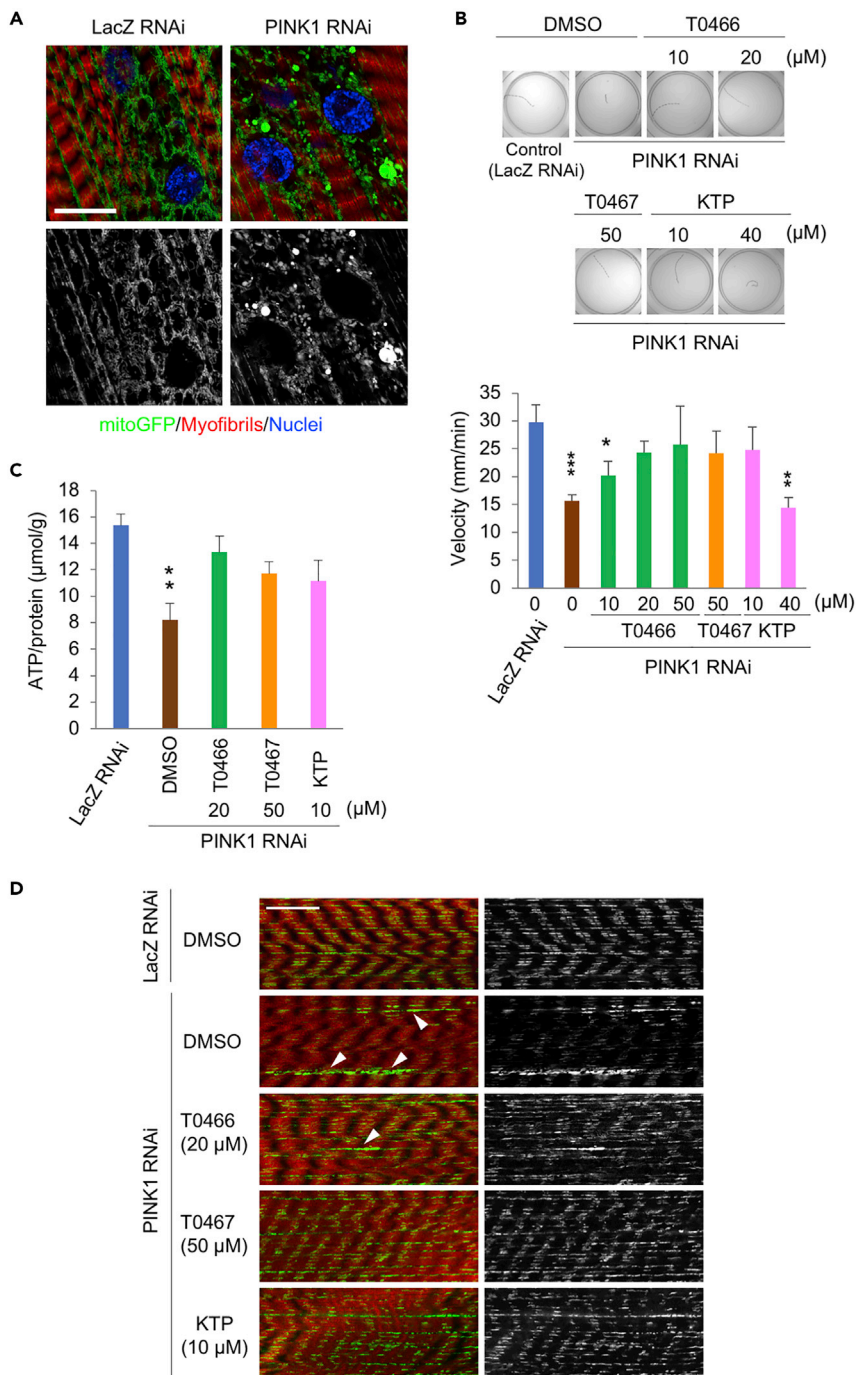
See also Figure S4.

**Figure 4. T0466 and T0467 Improve the Locomotion Defects Caused by the Reduced PINK1 Activity in *Drosophila***

(A) Mitochondrial morphological changes caused by PINK1 inactivation in the larval body-wall muscles. Mitochondria were visualized by mitoGFP (green). Myofibrils and nuclei were stained with TRITC-phalloidin (red) and DAPI (blue), respectively. Scale bar, 20 μm.

(B) Reduced PINK1 activity-mediated locomotion deficiency is mitigated by T0466 and T0467. Third-instar larvae treated with DMSO or the indicated drugs were placed in the center of 100-mm-diameter dishes and their movement recorded over 2 min using a CCD camera (images). The velocity over the last minute was graphed (mean ± SEM, n = 6–27 flies each). *p < 0.05, **p < 0.01, ***p < 0.0001 versus LacZ RNAi by Dunnett's test.

**Figure 4. Continued**

(C) ATP production in PINK1 RNAi flies is improved by T0466 and T0467 as well as KTP. ATP concentration was determined in the whole bodies of the third-instar larvae, normalizing with that of tissue soluble proteins. **p < 0.001 versus LacZ RNAi by Dunnett's test (mean ± SEM, n = 8 flies each).

(D) Mitochondrial aggregation in larval body-wall muscles caused by PINK1 inactivation was improved after the administration of T0466, T0467, or KTP. Mitochondria were visualized by mitoGFP (green) and counterstained with TRITC-phalloidin (red). Single channel images of mitoGFP are also shown (grayscale). Typical mitochondrial phenotypes observed in *PINK1 RNAi* flies are reduced mitoGFP signals and aggregated mitochondria (arrowheads). Scale bar, 20 μm. Genotypes used here are *UAS-LacZ RNAi/+; MHC-GAL4/UAS-mitoGFP* (LacZ RNAi) and *MHC-GAL4, UAS-PINK1 RNAi/ UAS-mitoGFP* (PINK1 RNAi).

See also Figures S5A and S5B.

Parkin-mediated mitophagy is proposed to be involved in cardiomyocyte development and prevents aging-related loss of muscle mass and strength (Chen and Dorn, 2013; Leduc-Gaudet et al., 2019). Mitochondrial translocation of GFP-Parkin was also observed in myoblasts at higher concentrations (>2.5 μM and >5 μM for T0466 and T0467, respectively) than those required in dopaminergic neurons (Figure 3D).

### T0466 and T0467 Mitigate Phenotypes Caused by Reduced PINK1 Activity in *Drosophila*

We assessed the effects of the two cpds on the PINK1-Parkin mitochondrial quality control pathway *in vivo*. Unlike rodent *PINK1* or *Parkin* models, *Drosophila* models exhibit obvious mitochondrial degeneration (Clark et al., 2006; Park et al., 2006; Yang et al., 2006). Flies do not consume any food or water for 3.5–4.5 days during pupation, making the evaluation of drug efficacy in adult flies just after eclosion difficult. We evaluated the efficacy of T0466, T0467, and KTP using larva, owing to their constant feeding behavior. We employed muscle-specific *PINK1* knockdown flies, which showed mitochondrial degeneration (Figure 4A and Videos S1 and S2) and locomotion defects at the third instar larval stage (Figure 4B). Inactivation of *PINK1* in the larval muscles affected crawling activity and reduced the velocity of locomotion to approximately 50% of that of control *LacZ* knockdown flies (Figure 4B). T0466 and T0467 significantly improved the locomotion defects in *PINK1* knockdown larvae (Figure 4B). KTP also mitigated the locomotion defects of *PINK1* knockdown larvae, but a higher dose of KTP did not (Figure 4B). ATP production in *PINK1* knockdown larvae was approximately 50% of that of *LacZ* knockdown flies and improved following T0466, T0467, and KTP administration (Figure 4C). In this context, both T0466 and T0467 did not affect the knockdown efficiency of PINK1 transcripts (Figure S5A), whereas these two cpds had a null effect on $PINK1^{-/-}$ flies (Figure S5B), strongly suggesting that the cpds mitigate mitochondrial dysfunction through the modulation of PINK1-Parkin signaling.

We examined the effects of drug administration on mitochondrial morphology and function in muscles. In normal control flies (LacZ RNAi, DMSO), the mitochondria of body-wall muscles were aligned alongside the myofibrils. However, in *PINK1* knockdown flies, aggregated or irregularly aligned mitochondria were observed (Figure 4D). Mitochondrial aggregation of body-wall muscles by PINK1 inactivation was partially ameliorated by T0466 treatment and markedly improved by T0467 and KTP (Figure 4D). A maintained proton gradient across the mitochondrial inner membrane is required for ATP-dependent $Ca^{2+}$ influx and efflux (Xing and Wu, 2018). We performed mitochondrial $Ca^{2+}$ imaging analysis using muscular mitochondria-targeted GCaMP in larval neuromuscular junctions. Sequential electrostimulation of motor neuron nerves in muscle-specific *PINK1* knockdown flies caused a gradual increase in GCaMP intensity baseline during five consecutive stimulations, indicating a delay in mitochondrial $Ca^{2+}$ efflux due to mitochondrial dysfunction (Figures 5A and S5C). Treatment with T0467 and KTP at concentrations most effectual in motor behavior analyses significantly improved the delay in mitochondrial $Ca^{2+}$ decay after the stimulation-mediated $Ca^{2+}$ spike, suggesting that T0467 and KTP alleviate PINK1 inactivation-induced mitochondrial dysfunction (Figures 5A and 5B).

We next examined whether these cpds exert a beneficial effect in dopaminergic neurons *in vivo*. Although *Drosophila* has an evolutionarily conserved blood-brain barrier (BBB), treatment with both cpds suppressed mitochondrial aggregates of larval dopaminergic neurons caused by PINK1 inactivation, suggesting that these drugs go through at least the *Drosophila* BBB (Figures 5C–5E) (Davis et al., 2019; Hindle et al., 2017; Limmer et al., 2014; Mayer et al., 2009; Zhang et al., 2018).

### DISCUSSION

Here, we describe a robust cell-based HTS for PINK1-Parkin signaling. Using this approach, we isolated two candidate cpds. Previous studies have reported two main kinds of drugs to activate PINK1, KTP (Hertz et al.,

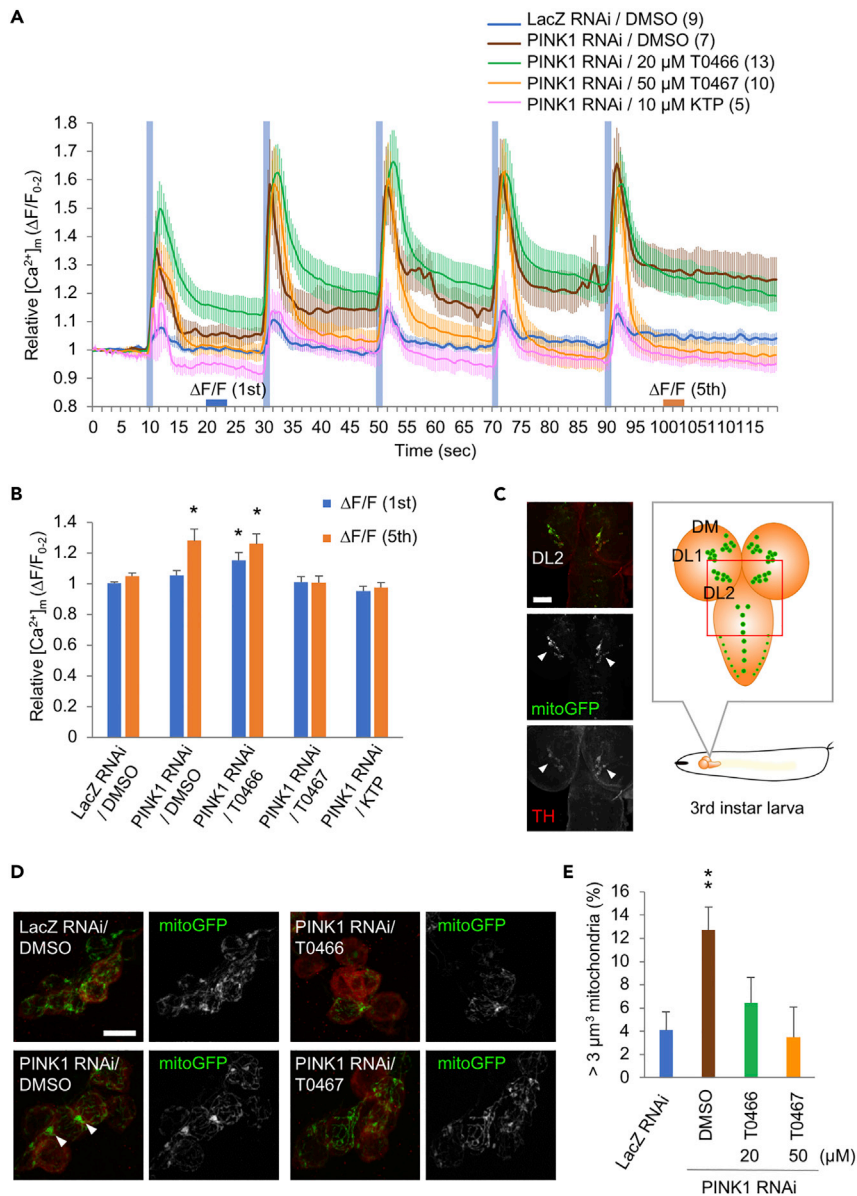**Figure 5. T0466 and T0467 Suppress the Mitochondrial Aggregation of Dopaminergic Neurons Caused by the Reduced PINK1 Activity in _Drosophila_**

(A and B) Reduced PINK1 activity-induced delay in mitochondrial $Ca^{2+}$ efflux is improved by T0467 and KTP. (A) Traces of relative fluorescence intensity changes before and after stimulations were graphed (n = 5–13 flies). Average fluorescence intensity showing mitochondrial $Ca^{2+}$ concentration ($[Ca^{2+}]_m$ from 0 to 2 s was set to 1. Blue bar indicates electrical stimulation (500 msec at 2.5 V). The number of samples analyzed are indicated in the graph legends. (B) Mitochondrial $Ca^{2+}$ decay after the first and fifth electrical stimulation (20–22 and 100–102 s) in (A). *p < 0.05 versus LacZ RNAi in each time window by Dunnett's test. Data are presented as mean $\pm$ SEM in (A) and (B).

(C) The DL2 clusters of dopaminergic neurons in the third-instar larval brain. (Left) The posterior brain of larva expressing mitoGFP (green) under the control of _TH-GAL4_ driver. The DL2 dopaminergic neurons (arrowheads) were also visualized with anti-TH (red). Scale bar, 50 μm. (Right) The position of the larval DL2 neuron clusters is depicted. The left images correspond to the red box region. DL, dorsolateral neurons; DM, dorsomedial neurons.

(D and E) Mitochondrial aggregates due to PINK1 inactivation are suppressed by T0466 and T0467. (D) The mitochondrial morphology (visualized by mitoGFP, green) of the DL2 cluster dopaminergic neurons (marked by anti-TH, red) treated with DMSO or the indicated drugs were imaged. Presented images were reconstructed from a series of z-stacked images (10–20 μm in depth). Scale bar, 10 μm. (E) Mitochondrial aggregates over 3 $\mu m^3$ (as shown by arrowheads in [D]) were graphed (n = 11–21 flies each). **p < 0.01 versus LacZ RNAi, DMSO using Dunnett's test.

**Figure 5. *Continued***
All transgenes were expressed by the *MHC-GAL4* (A, B) and *TH-GAL4* drivers (C–E).
See also Figure S5C.

2013) and its derivative (Osgerby et al., 2017) and niclosamide and its analogues (Barini et al., 2018). KTP is an ATP analogue that might affect a wide range of kinases and specific types of mRNA splicing (Lee et al., 2009; Wei et al., 2018). The niclosamide anthelmintic drug decreased the $\Delta\Psi$m, leading to PINK1 accumulation. In contrast, T0466 and T0467 do not appear to act directly on PINK1 and have unique potential for application as therapeutic reagents in diseases associated with mitochondrial degeneration.

OPA1 processing status revealed that T0466 affected $\Delta\Psi$m at concentrations >1 μM in dopaminergic neurons and HeLa cells. However, PINK1 levels at T0466 concentrations $\geq$1 μM were comparable with those of healthy controls. More uniquely, T0467 successfully activated mitochondrial translocation in dopaminergic neurons and myoblasts derived from iPSCs without obvious $\Delta\Psi$m reduction at lower concentrations than in HeLa/GFP-Parkin cells. Moreover, these two cpds reduced the levels of the mitochondrial unfolded protein $\Delta$OTC without $\Delta\Psi$m reduction-induced PINK1 accumulation.

T0466 and T0467 did not show obvious toxicity in *Drosophila* at concentrations <50 μM. All cpds examined mitigated the PINK1 inactivation-mediated larval locomotion defects and mitochondrial morphological defects and reduced ATP production. Additionally, T0467 and KTP improved the mitochondrial $Ca^{2+}$ response in *Drosophila* larval muscles. A recent study reported that KTP did not show beneficial effects in *PINK1* mutant mouse models, although appropriate evaluation was difficult owing to lack of PD-like phenotypes (Orr et al., 2017). Given the limitations of drug evaluation using rodent genetic PD models, our approach using a combination of dopaminergic neuron cultures from iPS cells and *Drosophila* genetic PD models could provide a new standard method to rapidly assess drug efficacy.

Dysfunction of Parkin-mediated mitochondrial maintenance is involved in the pathophysiological basis of a variety of diseases including PD, amyotrophic lateral sclerosis, diabetes, cardiomyopathy, and muscular atrophy (Billia et al., 2011; Hoshino et al., 2014; Kang et al., 2018; Kitada et al., 1998; Leduc-Gaudet et al., 2019; Palomo et al., 2018). Heterozygous mutations in PINK1 and Parkin are a reported risk for sporadic PD (Klein et al., 2007; Shulskaya et al., 2017). Previously, we reported that PINK1-Parkin activity is higher in dopaminergic neurons than in other cells differentiated from the same iPSC lines (Shiba-Fukushima et al., 2017). Thus, the cpds identified in this study might be especially effective in dopaminergic neurons affected in PD. Further studies should elucidate the molecular mechanism underlying the activation of the PINK1-Parkin pathway by these cpds. Moreover, drug optimization, including structural optimization to reduce toxicity and enhance delivery to the central nervous system, is expected to accelerate the clinical development of drugs to treat PD and related diseases.

## Limitations of the Study

Herein, we developed a cell-based screening system for cpds that activate PINK1-Parkin signaling and identified two cpds. Although these cpds are effective in mammalian cells and *Drosophila* in the presence of PINK1, this study did not determine the molecular targets of these cpds. Thus, the establishment of non-human primate models of PINK1-Parkin-associated PD that reproduce PD-like phenotypes and the evaluation of drug properties including pharmacokinetic profiles and potential adverse effects using these mammalian models are required in the future studies.

## METHODS

All methods can be found in the accompanying Transparent Methods supplemental file.

## DATA AND CODE AVAILABILITY

The data that support the findings of this study are available from the corresponding author upon reasonable request.

## SUPPLEMENTAL INFORMATION

Supplemental Information can be found online at https://doi.org/10.1016/j.isci.2020.101048.

## ACKNOWLEDGMENTS

## AUTHOR CONTRIBUTIONS

Conceptualization, K.S-F. and Y.I.; Methodology, K.S-F., T.I., and Y.I.; Investigation, KS-F., T.I., O.S., and H.I.; Visualization, K.S-F., T.I., O.S., and Y.I.; Writing original draft, K.S-F. and Y.I.; Funding acquisition, K.S-F., Y.I., and N.H.; Resources, K-i.I., H.O., and W.A.; Supervision, N.H.

## DECLARATION OF INTERESTS

The authors declare that they have no conflict of interest.

## REFERENCES

Akabane, S., Uno, M., Tani, N., Shimazaki, S., Ebara, N., Kato, H., Kosako, H., and Oka, T. (2016). PKA regulates PINK1 stability and parkin recruitment to damaged mitochondria through phosphorylation of MIC60. Mol. Cell 62, 371–384.

Barini, E., Miccoli, A., Tinarelli, F., Mulholland, K., Kadri, H., Khanim, F., Stojanovski, L., Read, K.D., Burness, K., Blow, J.J., et al. (2018). The anthelmintic drug niclosamide and its analogues activate the Parkinson's disease associated protein kinase PINK1. Chembiochem 19, 425–429.

Billia, F., Hauck, L., Konecny, F., Rao, V., Shen, J., and Mak, T.W. (2011). PTEN-inducible kinase 1 (PINK1)/Park6 is indispensable for normal heart function. Proc. Natl. Acad. Sci. U S A 108, 9572–9577.

Chen, Y., and Dorn, G.W. (2013). PINK1-phosphorylated mitofusin 2 is a Parkin receptor for culling damaged mitochondria. Science 340, 471–475.

Clark, I.E., Dodson, M.W., Jiang, C., Cao, J.H., Huh, J.R., Seol, J.H., Yoo, S.J., Hay, B.A., and Guo, M. (2006). Drosophila pink1 is required for mitochondrial function and interacts genetically with parkin. Nature 441, 1162–1166.

Dar, A.C., and Shokat, K.M. (2011). The evolution of protein kinase inhibitors from antagonists to agonists of cellular signaling. Annu. Rev. Biochem. 80, 769–795.

Davis, M.J., Talbot, D., and Jemc, J. (2019). Assay for blood-brain barrier integrity in Drosophila melanogaster. J. Vis. Exp. 151, e60233.

Deng, H., Dodson, M.W., Huang, H., and Guo, M. (2008). The Parkinson's disease genes pink1 and parkin promote mitochondrial fission and/or

inhibit fusion in Drosophila. Proc. Natl. Acad. Sci. U S A 105, 14503–14508.

England, C.G., Ehlerding, E.B., and Cai, W. (2016). NanoLuc: a small luciferase is brightening up the field of bioluminescence. Bioconjug. Chem. 27, 1175–1187.

Heo, J.M., Ordureau, A., Paulo, J.A., Rinehart, J., and Harper, J.W. (2015). The PINK1-PARKIN mitochondrial ubiquitylation pathway drives a program of OPTN/NDP52 recruitment and TBK1 activation to promote mitophagy. Mol. Cell 60, 7–20.

Hertz, N.T., Berthet, A., Sos, M.L., Thorn, K.S., Burlingame, A.L., Nakamura, K., and Shokat, K.M. (2013). A neo-substrate that amplifies catalytic activity of Parkinson's-disease-related kinase PINK1. Cell 154, 737–747.

Hildebrand, J.M., Tanzer, M.C., Lucet, I.S., Young, S.N., Spall, S.K., Sharma, P., Pierotti, C., Garnier, J.M., Dobson, R.C., Webb, A.I., et al. (2014). Activation of the pseudokinase MLKL unleashes the four-helix bundle domain to induce membrane localization and necroptotic cell death. Proc. Natl. Acad. Sci. U S A 111, 15072–15077.

Hindle, S.J., Munji, R.N., Dolghih, E., Gaskins, G., Orng, S., Ishimoto, H., Soung, A., DeSalvo, M., Kitamoto, T., Keiser, M.J., et al. (2017). Evolutionarily conserved roles for blood-brain barrier xenobiotic transporters in endogenous steroid partitioning and behavior. Cell Rep. 21, 1304–1316.

Hoshino, A., Ariyoshi, M., Okawa, Y., Kaimoto, S., Uchihashi, M., Fukai, K., Iwai-Kanai, E., Ikeda, K., Ueyama, T., Ogata, T., et al. (2014). Inhibition of p53 preserves Parkin-mediated mitophagy and pancreatic beta-cell function in diabetes. Proc. Natl. Acad. Sci. U S A 111, 3116–3121.

Ishihara, N., Fujita, Y., Oka, T., and Mihara, K. (2006). Regulation of mitochondrial morphology through proteolytic cleavage of OPA1. EMBO J. 25, 2966–2977.

Jin, S.M., Lazarou, M., Wang, C., Kane, L.A., Narendra, D.P., and Youle, R.J. (2010). Mitochondrial membrane potential regulates PINK1 import and proteolytic destabilization by PARL. J. Cell Biol. 191, 933–942.

Jin, S.M., and Youle, R.J. (2013). The accumulation of misfolded proteins in the mitochondrial matrix is sensed by PINK1 to induce PARK2/Parkin-mediated mitophagy of polarized mitochondria. Autophagy 9, 1750–1757.

Kane, L.A., Lazarou, M., Fogel, A.I., Li, Y., Yamano, K., Sarraf, S.A., Banerjee, S., and Youle, R.J. (2014). PINK1 phosphorylates ubiquitin to activate Parkin E3 ubiquitin ligase activity. J. Cell Biol. 205, 143–153.

Kang, C., Badr, M.A., Kyrychenko, V., Eskelinen, E.-L., and Shirokova, N. (2018). Deficit in PINK1/PARKIN-mediated mitochondrial autophagy at late stages of dystrophic cardiomyopathy. Cardiovasc. Res. 114, 90–102.

Kitada, T., Asakawa, S., Hattori, N., Matsumine, H., Yamamura, Y., Minoshima, S., Yokochi, M., Mizuno, Y., and Shimizu, N. (1998). Mutations in the parkin gene cause autosomal recessive juvenile parkinsonism. Nature 392, 605–608.

Klein, C., Lohmann-Hedrich, K., Rogaeva, E., Schlossmacher, M.G., and Lang, A.E. (2007). Deciphering the role of heterozygous mutations in genes associated with parkinsonism. Lancet Neurol. 6, 652–662.

Kondapalli, C., Kazlauskaite, A., Zhang, N., Woodroof, H.I., Campbell, D.G., Gourlay, R., Burchell, L., Walden, H., Macartney, T.J., Deak,

M., et al. (2012). PINK1 is activated by mitochondrial membrane potential depolarization and stimulates Parkin E3 ligase activity by phosphorylating Serine 65. Open Biol. *2*, 120080.

Koyano, K., Okatsu, K., Kosako, H., Tamura, Y., Go, E., Kimura, M., Kimura, Y., Tsuchiya, H., Yoshihara, H., Hirokawa, T., et al. (2014). Ubiquitin is phosphorylated by PINK1 to activate parkin. Nature *510*, 162–166.

Leduc-Gaudet, J.P., Reynaud, O., Hussain, S.N., and Gouspillou, G. (2019). Parkin overexpression protects from ageing-related loss of muscle mass and strength. J. Physiol. *597*, 1975–1991.

Lee, G., Papapetrou, E.P., Kim, H., Chambers, S.M., Tomishima, M.J., Fasano, C.A., Ganat, Y.M., Menon, J., Shimizu, F., Viale, A., et al. (2009). Modelling pathogenesis and treatment of familial dysautonomia using patient-specific iPSCs. Nature *461*, 402–406.

Limmer, S., Weiler, A., Volkenhoff, A., Babatz, F., and Klambt, C. (2014). The Drosophila blood-brain barrier: development and function of a glial endothelium. Front. Neurosci. *8*, 365.

Liu, S., Sawada, T., Lee, S., Yu, W., Silverio, G., Alapatt, P., Millan, I., Shen, A., Saxton, W., Kanao, T., et al. (2012). Parkinson's disease-associated kinase PINK1 regulates Miro protein level and axonal transport of mitochondria. PLoS Genet. *8*, e1002537.

Ma, B., Marcotte, D., Paramasivam, M., Michelsen, K., Wang, T., Bertolotti-Ciarlet, A., Jones, J.H., Moree, B., Butko, M., Salafsky, J., et al. (2016). ATP-competitive MLKL binders have no functional impact on necroptosis. PLoS One *11*, e0165983.

Matsuda, N., Sato, S., Shiba, K., Okatsu, K., Saisho, K., Gautier, C.A., Sou, Y.S., Saiki, S., Kawajiri, S., Sato, F., et al. (2010). PINK1 stabilized by mitochondrial depolarization recruits Parkin to damaged mitochondria and activates latent Parkin for mitophagy. J. Cell Biol. *189*, 211–221.

Matsumoto, G., Shimogori, T., Hattori, N., and Nukina, N. (2015). TBK1 controls autophagosomal engulfment of polyubiquitinated mitochondria through p62/SQSTM1 phosphorylation. Hum. Mol. Genet. *24*, 4429–4442.

Mayer, F., Mayer, N., Chinn, L., Pinsonneault, R.L., Kroetz, D., and Bainton, R.J. (2009). Evolutionary conservation of vertebrate blood-brain barrier chemoprotective mechanisms in Drosophila. J. Neurosci. *29*, 3538–3550.

Narendra, D.P., Jin, S.M., Tanaka, A., Suen, D.F., Gautier, C.A., Shen, J., Cookson, M.R., and Youle, R.J. (2010). PINK1 is selectively stabilized on impaired mitochondria to activate Parkin. PLoS Biol. *8*, e1000298.

Okatsu, K., Kimura, M., Oka, T., Tanaka, K., and Matsuda, N. (2015). Unconventional PINK1 localization to the outer membrane of depolarized mitochondria drives Parkin recruitment. J. Cell Sci. *128*, 964–978.

Ordureau, A., Sarraf, S.A., Duda, D.M., Heo, J.M., Jedrychowski, M.P., Sviderskiy, V.O., Olszewski, J.L., Koerber, J.T., Xie, T., Beausoleil, S.A., et al. (2014). Quantitative proteomics reveal a feedforward mechanism for mitochondrial PARKIN translocation and ubiquitin chain synthesis. Mol. Cell *56*, 360–375.

Orr, A.L., Rutaganira, F.U., de Roulet, D., Huang, E.J., Hertz, N.T., Shokat, K.M., and Nakamura, K. (2017). Long-term oral kinetin does not protect against alpha-synuclein-induced neurodegeneration in rodent models of Parkinson's disease. Neurochem. Int. *109*, 106–116.

Osgerby, L., Lai, Y.C., Thornton, P.J., Amalfitano, J., Le Duff, C.S., Jabeen, I., Kadri, H., Miccoli, A., Tucker, J.H.R., Muqit, M.M.K., et al. (2017). Kinetin riboside and its protides activate the Parkinson's disease associated PTEN-induced putative kinase 1 (PINK1) independent of mitochondrial depolarization. J. Med. Chem. *60*, 3518–3524.

Palomo, G.M., Granatiero, V., Kawamata, H., Konrad, C., Kim, M., Arreguin, A.J., Zhao, D., Milner, T.A., and Manfredi, G. (2018). Parkin is a disease modifier in the mutant SOD1 mouse model of ALS. EMBO Mol. Med. *10*, e8888.

Park, J., Lee, S.B., Lee, S., Kim, Y., Song, S., Kim, S., Bae, E., Kim, J., Shong, M., Kim, J.M., et al. (2006). Mitochondrial dysfunction in Drosophila PINK1 mutants is complemented by parkin. Nature *441*, 1157–1161.

Pickrell, A.M., Huang, C.H., Kennedy, S.R., Ordureau, A., Sideris, D.P., Hoekstra, J.G., Harper, J.W., and Youle, R.J. (2015). Endogenous parkin preserves dopaminergic substantia nigral neurons following mitochondrial DNA mutagenic stress. Neuron *87*, 371–381.

Pimenta de Castro, I., Costa, A.C., Lam, D., Tufi, R., Fedele, V., Moisoi, N., Dinsdale, D., Deas, E., Loh, S.H., and Martins, L.M. (2012). Genetic analysis of mitochondrial protein misfolding in *Drosophila melanogaster*. Cell Death Differ. *19*, 1308–1316.

Richter, B., Sliter, D.A., Herhaus, L., Stolz, A., Wang, C., Beli, P., Zaffagnini, G., Wild, P., Martens, S., Wagner, S.A., et al. (2016). Phosphorylation of OPTN by TBK1 enhances its binding to Ub chains and promotes selective autophagy of damaged mitochondria. Proc. Natl. Acad. Sci. U S A *113*, 4039–4044.

Shiba-Fukushima, K., Arano, T., Matsumoto, G., Inoshita, T., Yoshida, S., Ishihama, Y., Ryu, K.Y., Nukina, N., Hattori, N., and Imai, Y. (2014). Phosphorylation of mitochondrial polyubiquitin by PINK1 promotes Parkin mitochondrial tethering. PLoS Genet. *10*, e1004861.

Shiba-Fukushima, K., Imai, Y., Yoshida, S., Ishihama, Y., Kanao, T., Sato, S., and Hattori, N. (2012). PINK1-mediated phosphorylation of the Parkin ubiquitin-like domain primes mitochondrial translocation of Parkin and regulates mitophagy. Sci. Rep. *2*, 1002.

Shiba-Fukushima, K., Ishikawa, K.I., Inoshita, T., Izawa, N., Takanashi, M., Sato, S., Onodera, O.,

Akamatsu, W., Okano, H., Imai, Y., et al. (2017). Evidence that phosphorylated ubiquitin signaling is involved in the etiology of Parkinson's disease. Hum. Mol. Genet. *26*, 3172–3185.

Shulskaya, M.V., Shadrina, M.I., Fedotova, E.Y., Abramycheva, N.Y., Limborska, S.A., Illarioshkin, S.N., and Slominsky, P.A. (2017). Second mutation in PARK2 is absent in patients with sporadic Parkinson's disease and heterozygous exonic deletions/duplications in parkin gene. Int. J. Neurosci. *127*, 781–784.

Tanaka, A., Cleland, M.M., Xu, S., Narendra, D.P., Suen, D.F., Karbowski, M., and Youle, R.J. (2010). Proteasome and p97 mediate mitophagy and degradation of mitofusins induced by Parkin. J. Cell Biol. *191*, 1367–1380.

Valente, E.M., Abou-Sleiman, P.M., Caputo, V., Muqit, M.M., Harvey, K., Gispert, S., Ali, Z., Del Turco, D., Bentivoglio, A.R., Healy, D.G., et al. (2004). Hereditary early-onset Parkinson's disease caused by mutations in PINK1. Science *304*, 1158–1160.

Wang, X., Winter, D., Ashrafi, G., Schlehe, J., Wong, Y.L., Selkoe, D., Rice, S., Steen, J., LaVoie, M.J., and Schwarz, T.L. (2011). PINK1 and Parkin target Miro for phosphorylation and degradation to arrest mitochondrial motility. Cell *147*, 893–906.

Wei, Y., Liu, D., Zheng, Y., Hao, C., Li, H., and Ouyang, W. (2018). Neuroprotective effects of kinetin against glutamate-induced oxidative cytotoxicity in HT22 cells: involvement of Nrf2 and heme oxygenase-1. Neurotox. Res. *33*, 725–737.

Xing, X., and Wu, C.F. (2018). Unraveling synaptic GCaMP signals: differential excitability and clearance mechanisms underlying distinct Ca(2+) dynamics in tonic and phasic excitatory, and aminergic modulatory motor terminals in Drosophila. eNeuro 5, https://doi.org/10.1523/ENEURO.0362-17.2018.

Yang, Y., Gehrke, S., Imai, Y., Huang, Z., Ouyang, Y., Wang, J.W., Yang, L., Beal, M.F., Vogel, H., and Lu, B. (2006). Mitochondrial pathology and muscle and dopaminergic neuron degeneration caused by inactivation of Drosophila Pink1 is rescued by Parkin. Proc. Natl. Acad. Sci. U S A *103*, 10793–10798.

Yang, Y., Ouyang, Y., Yang, L., Beal, M.F., McQuibban, A., Vogel, H., and Lu, B. (2008). Pink1 regulates mitochondrial dynamics through interaction with the fission/fusion machinery. Proc. Natl. Acad. Sci. U S A *105*, 7070–7075.

Zhang, S.L., Yue, Z., Arnold, D.M., Artiushin, G., and Sehgal, A. (2018). A circadian clock in the blood-brain barrier regulates xenobiotic efflux. Cell *173*, 130–139 e110.

Ziviani, E., Tao, R.N., and Whitworth, A.J. (2010). Drosophila parkin requires PINK1 for mitochondrial translocation and ubiquitinates mitofusin. Proc. Natl. Acad. Sci. U S A *107*, 5018–5023.

# Supplemental Information

# A Cell-Based High-Throughput Screening

# Identified Two Compounds

# that Enhance PINK1-Parkin Signaling

Kahori Shiba-Fukushima, Tsuyoshi Inoshita, Osamu Sano, Hidehisa Iwata, Kei-ichi Ishikawa, Hideyuki Okano, Wado Akamatsu, Yuzuru Imai, and Nobutaka Hattori
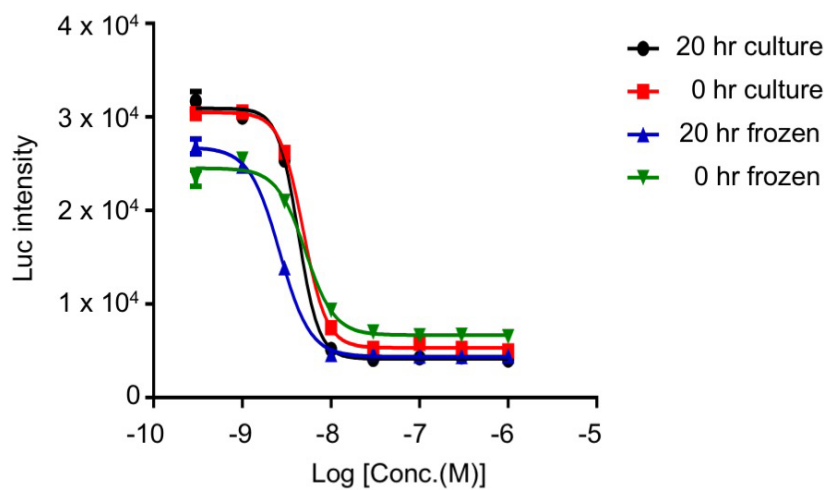
**Figure S1. Validation of HTS method using suspension culture, Related to Figure 1.**
The NL-Mfn1 reporter assay works using cell suspensions. Reporter cells were treated with valinomycin (Val) under four different culture conditions. Reporter assays were performed 3 h after Val addition. For the 20 h culture, growing cells on dishes were plated and cultured for 20 h before the addition of Val. For the 0 h culture, growing cells on dishes were plated and immediately treated with Val. For the 20 h frozen treatment, frozen cells were plated and cultured for 20 h before the addition of Val. For the 0 h frozen treatment, frozen cells were plated and immediately treated with Val. Data are presented as mean ± SD from 2 independent samples.
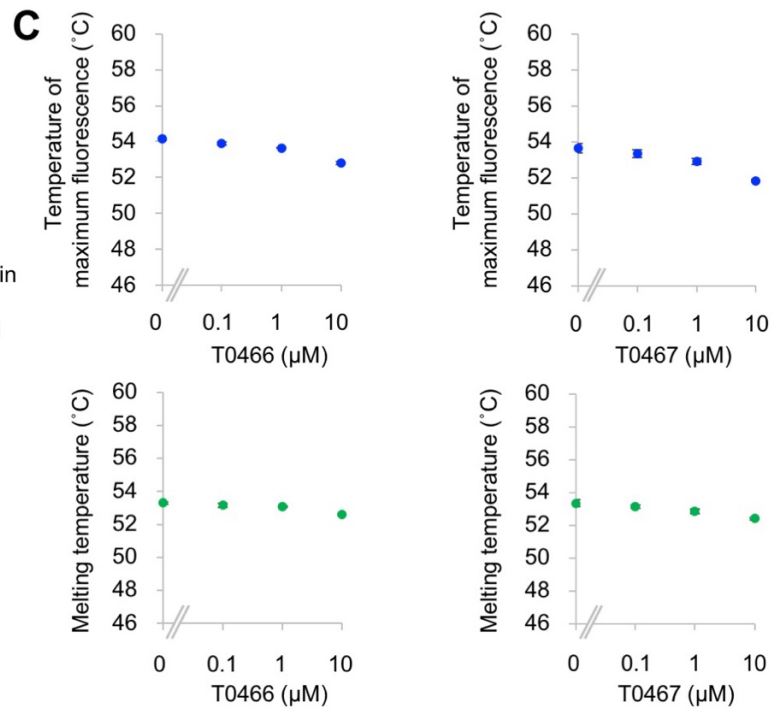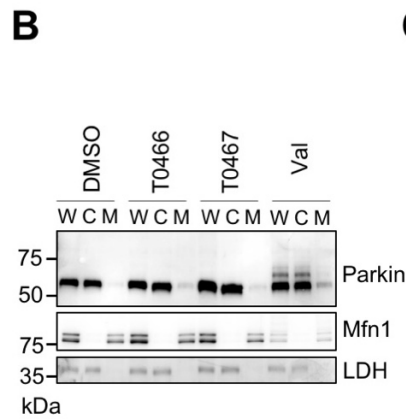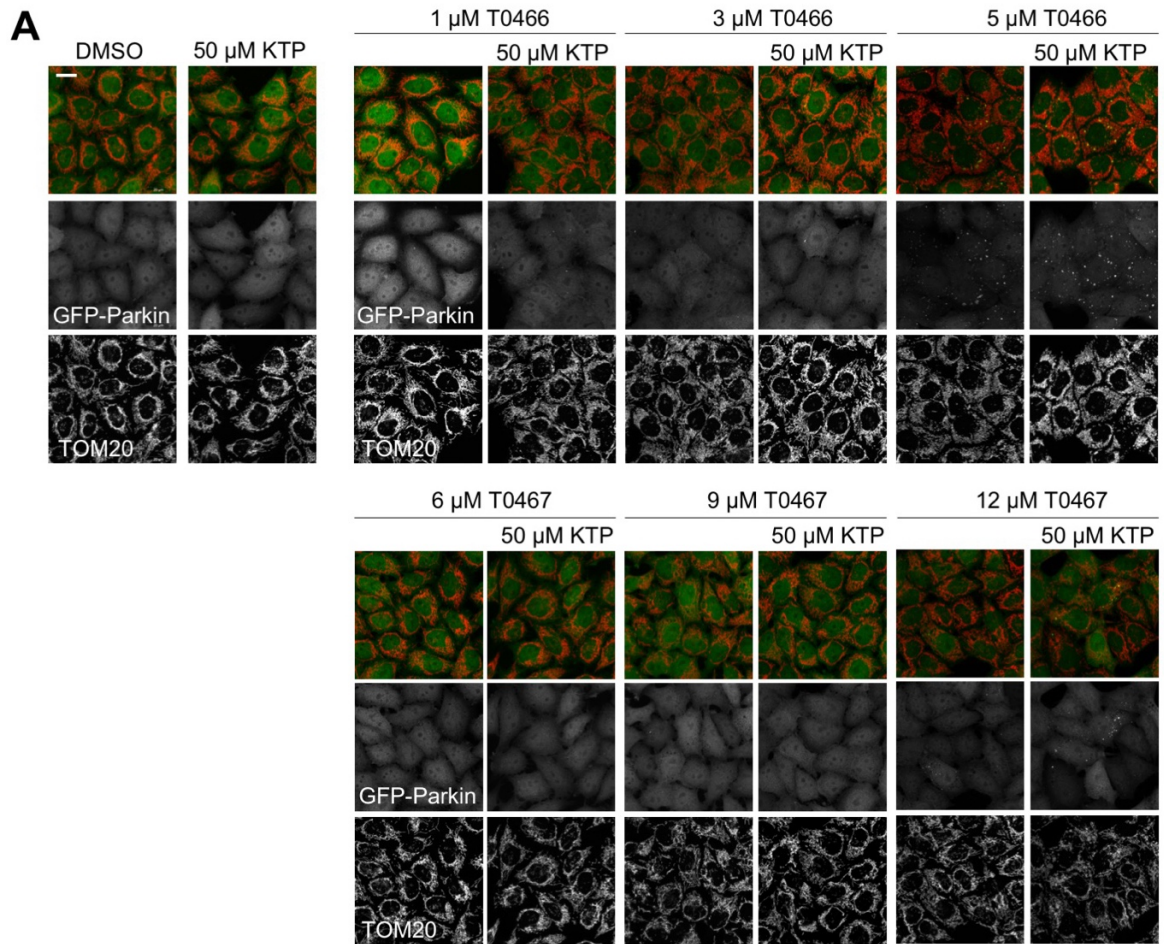
# A



# B



# C

**Figure S2. Titration of T0466 and T0467 with or without KTP, Related to Figure 2.**

(**A**) KTP does not potentiate the effects of T0466 and T0467 on Parkin activation. HeLa/GFP-Parkin cells were treated with T0466 and T0467 with or without 50 µM KTP at the indicated concentrations for 8 h. Treatment with 5 µM T0466 or 12 µM T0467 activated Parkin, detected as punctate GFP signals, while KTP alone did not. Mitochondria were visualized with anti-TOM20 staining. Scale bar = 20 µm.

(**B**) Biochemical fractionation of mitochondrial Parkin after drug treatment. HeLa/GFP-Parkin cells were treated with DMSO, 5 µM T0466, 20 µM T0467, or 20 µM Val for 3 h. W, whole lysate; C, cytosolic fraction; M, mitochondrial fraction. Mfn1 and Lactate dehydrogenase (LDH) served as mitochondria and cytosol markers, respectively.

(**C**) No evidence that Parkin is a target of cpds was seen. Upper graphs (mean ± SEM, n = 4 technical replicates) indicate the temperature of maximum fluorescence of SYPRO Orange at given concentrations of cpds in the thermal shift assay of Parkin. Lower graphs (mean ± SEM, n = 4 technical replicates) indicate melting temperature obtained by the first derivative of the fluorescence intensity curves. Here, 0 µM means solvent DMSO alone. The addition of cpds to Parkin did not result in a prominent shift in the temperature of the melt peak, suggesting that cpds do not bind to Parkin.
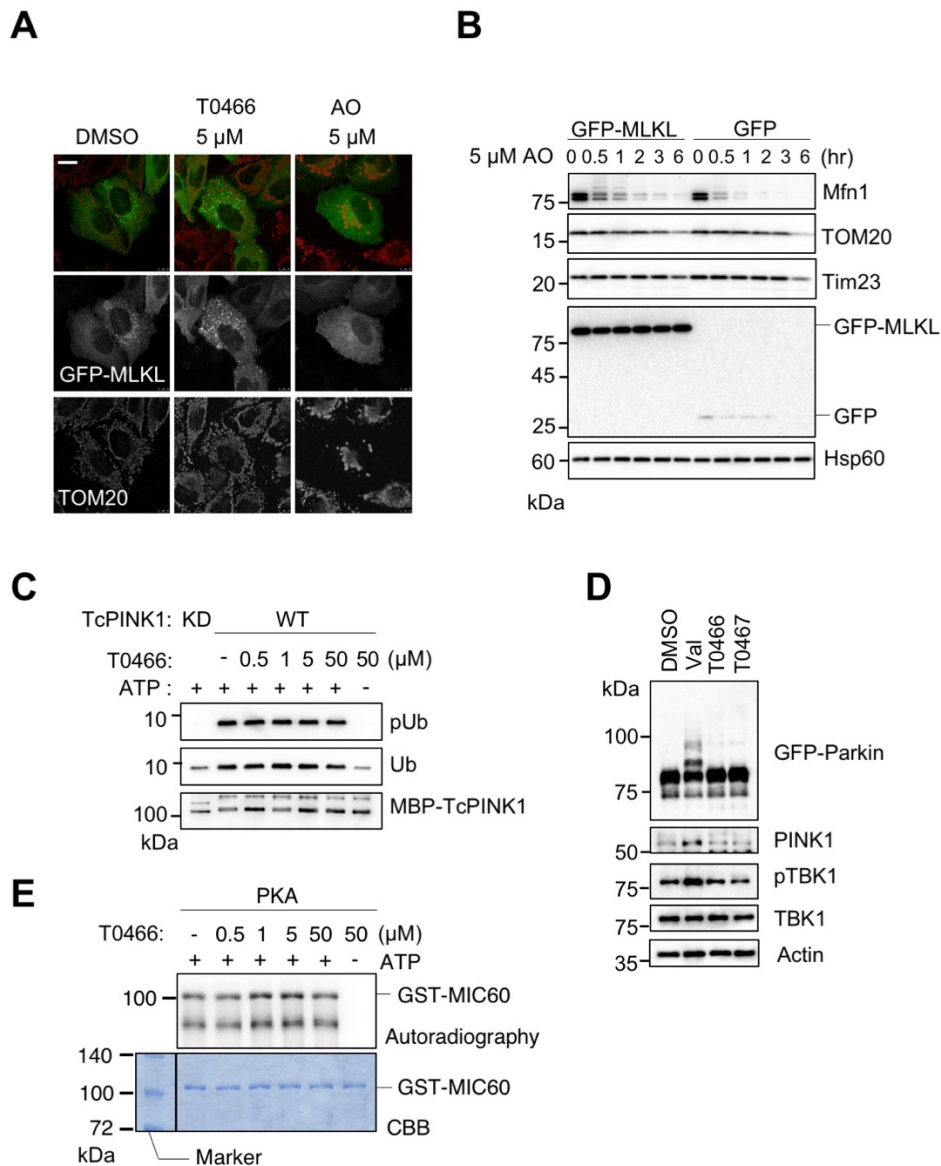
**Figure S3. PINK1, TBK1, and PKA are not T0466 or T0467 targets, Related to Figure 2.**
(**A**) T0466 does not alter MLKL subcellular localization. HeLa cells transfected with GFP-MLKL were treated with T0466 (5 µM) or AO (5 µM) for 3 h. Scale bar = 20 µm.
(**B**) MLKL does not affect Parkin-mediated mitophagy. Cells expressing GFP-MLKL or GFP were treated with 5 µM AO for the indicated times.
(**C**) T0466 does not modulate the kinase activity of PINK1. Recombinant TcPINK1 was preincubated with or without T0466 for 30 min at RT and further incubated with Ubiquitin (Ub) at 30˚C for 90 min in the presence or absence of 2 mM ATP. Phosphorylation of Ub at Ser65 (pUb) was detected with anti-phospho-Ser65 Ub antibody.
(**D**) T0466 and T0467 do not stimulate PINK1 accumulation and TBK1 phosphorylation. HeLa/GFP-Parkin cells were treated with 5 µM T0466 and T0467 for 3 h. The indicated proteins were analyzed by western blot.
(**E**) T0466 does not modulate PKA kinase activity. PKA was preincubated with or without T0466 for 30 min at RT and further incubated with GST-MIC60 at 30˚C for 90 min in the presence or absence of $\gamma$-$^{32}$P ATP. Phosphorylation of GST-MIC60 was detected by autoradiography. The amounts of GST-MIC60 were detected by Coomassie brilliant blue (CBB) staining.
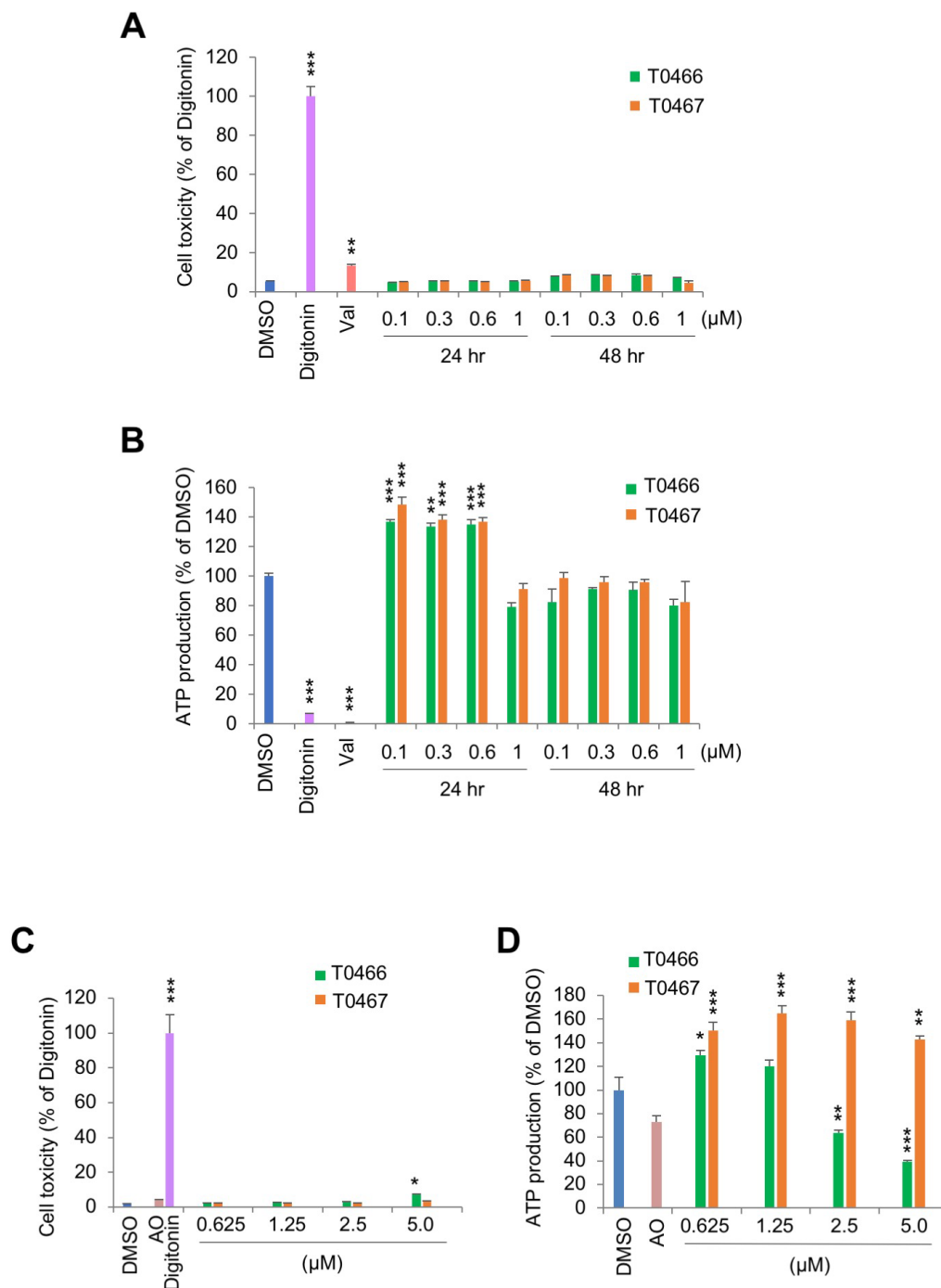
**Figure S4. Effects of T0466 and T0467 on ATP production and cell toxicity in dopaminergic neuron culture, Related to Figure 3.**

(**A**) Cell toxicity test of chemicals in dopaminergic neuron culture treated with chemicals at concentrations of 0.1−1 μM for the indicated times (mean ± SEM, n = 4 independent samples). DMSO and digitonin treatments served as mock and positive controls, respectively. Valinomycin (Val, 2 μM) was also put as a mitochondrial toxin treatment. **$p < 0.005$, ***$p < 0.0001$ *vs*. DMSO by one-way ANOVA with Tukey-Kramer test.

(**B**) ATP measurement in iPSC-derived dopaminergic neuron culture treated with chemicals at concentrations of 0.1-1 μM for the indicated times (mean ± SEM, n = 4 independent samples). Valinomycin (Val, 2 μM) treatment served a mitochondrial toxin control. **$p < 0.01$, ***$p < 0.001$ *vs.* DMSO by one-way ANOVA with Tukey-Kramer test.

(**C**) Cell toxicity test of chemicals in dopaminergic neuron culture treated with chemicals at concentrations of 0.625-5 μM for 8 h (mean ± SEM, n = 4-6 independent samples). DMSO and digitonin treatments served as mock and positive controls, respectively. AO (2 μM each) treatment served a mitochondrial toxin control. *$p < 0.05$, ***$p < 0.0001$ *vs.* DMSO by one-way ANOVA with Tukey-Kramer test.

(**D**) ATP measurement in iPSC-derived dopaminergic neuron culture treated with chemicals at concentrations of 0.625-5 μM for 8 h (mean ± SEM, n = 4-6 independent samples). *$p < 0.05$, **$p < 0.01$, ***$p < 0.0001$ *vs.* DMSO by one-way ANOVA with Tukey-Kramer test.
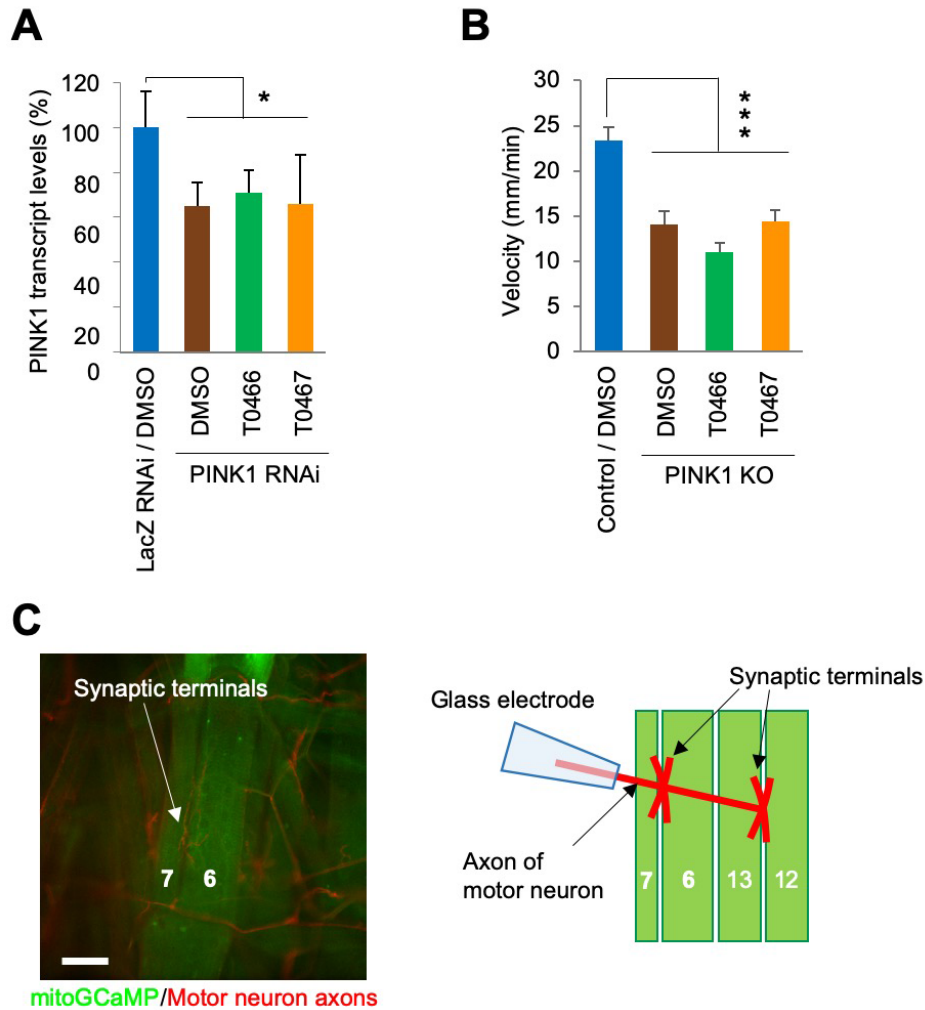
**Figure S5. Mitochondrial defects in the muscles of PINK1 knockdown larvae, Related to Figures 4 and 5.**

(**A**) T0466 and T0467 do not affect PINK1 knockdown efficiency. *PINK1* transcript levels normalized with housekeeping *RP49* levels in the larval body-wall muscles are represented (mean ± SEM, n = 5 biological replicates). *$p < 0.05$ using Dunnett's test.

(**B**) T0466 and T0467 do not improve the locomotion of PINK1 KO flies. The locomotion of PINK1 KO third-instar larvae treated with DMSO or the indicated drugs were recorded as in Fig. 4B and graphed (mean ± SEM, n = 11–14 flies each). ***$p < 0.0001$ using one-way ANOVA with Tukey-Kramer test.

(**C**) Larval body-wall muscles six and seven at the abdominal segment three and motor neuron axons projected to these muscles are shown. Motor neuron axons were visualized with Alexa594 conjugated anti-HRP (red). Bar = 100 μm. (right) Diagram of the mitochondrial Ca$^{2+}$ imaging experiment. Motor neuron axons projecting into abdominal segment three muscles are stimulated by a glass suction electrode with a stimulation for 500 msec 5 times at 20 sec intervals.

Genotypes are: (**A, C**) *UAS-LacZ RNAi/+; MHC-GAL4/UAS-mitoGFP* (LacZ RNAi) and *MHC-GAL4, UAS-PINK1 RNAi/UAS-mitoGFP* (PINK1 RNAi), (**B**) *+/Y; +/+; MHC-GAL4, UAS-mitoGFP/+* (Control), *PINK1$^{B9}$/Y; +/+; MHC-GAL4, UAS-mitoGFP/+* (PINK1 KO). Males were discriminated by their testes.

**Transparent Methods**

**Plasmids and cell lines**
pNLF1-C (Promega) and pMXs-puro/-neo (Cell Biolabs) vectors were purchased. Complementary DNA of Human Mfn1 amplified from HeLa cells was cloned into the XhoI and NotI sites of the pCAGGS-CFP vector (a gift of Dr. Y. Ohba at Hokkaido University). The NL coding sequence was retrieved from pNLF1-C as an EcoRI/XhoI fragment. NL and Mfn1 fragments were then cloned into the EcoRI and NotI sites of the pMXs-puro vector. Human Parkin cDNA was cloned into the EcoRI and XbaI sites of pMXs-neo vector. HeLa cells were transfected with pMXs-puro-NL-Mfn1 and pMXs-neo-Parkin or pMXs-neo empty vector along with pcDNA3-Hyg-mSlc7a1-VSVG. Stable cell lines were selected with 1 μg/ml puromycin and 1 mg/ml neomycin (Shiba-Fukushima et al., 2012). Single clones stably expressing the NL-Mfn1 reporter, with or without Parkin, were then isolated and characterized. HeLa cell/NL-Mfn1/Parkin and HeLa cell/NL-Mfn1/Vector were used for HTS and counter screening, respectively. MLKL cDNA amplified from HeLa cells was cloned into the XhoI and BamHI sites of pEGFP-C1 vector. GFP-Parkin was inserted into the lentivirus vector pLVSIN-CMV-Pur for neuronal transfection (Takara Bio, Japan). HeLa cells stably expressing GFP-Parkin (HeLa/GFP-Parkin cells) were generated by retroviral infection of pMXs-puro-GFP-Parkin WT along with pcDNA3-Hyg-mSlc7a1-VSVG (Shiba-Fukushima et al., 2014). pGEX4T-MIC60 (Akabane et al., 2016) was kindly provided by Drs. T. Oka (Rikkyo University). $PINK1^{-/-}$ HeLa cell line (Kane et al., 2014) and ΔOTC/HeLa-Tet On cell line (Jin and Youle, 2013) were kindly provided by R. Youle (NIH).

**Drug discovery screening**
The Takeda cpd library (~45,000 cpds) was plated onto 1536-well plates using an Echo 555 liquid handler (Labcyte). The reporter cell suspension (5 μl; 5 x $10^5$ cells/ml) was dispensed onto 1536-well plates using a Multidrop Combi (Thermo Fisher Scientific). The plates were incubated for 3 h at 37˚C. DMSO and 1 μM val were included in every plate as negative and positive controls, respectively. Cell viability was monitored using CellTiter-Fluor Cell Viability Assay reagents (Promega) and NL activity was sequentially measured using the Nano-Glo Luciferase Assay System (Promega). Plate readings for the HTS were performed using EnVison (PerkinElmer). The chemiluminescence signal intensities (NL activity) was normalized using fluorescence (cell density) and the candidates were subjected to a dose-response test (at 0.3, 3, and 10 μM). Cpds showing over 30% reduction from the negative control (DMSO) in the Parkin-expressing cells were further tested using an adherent cell format with different doses (3 and 10 μM). The resultant 31 cpds were further subjected to ΔΨm testing using 10 nM MitoTracker Red CMXRos (Thermo Fisher Scientific). Two cpds with ≤ 10% ΔΨm changes at 3 μM were selected.

**Antibodies and reagents**
The following antibodies were used for western blotting: anti-phospho-Ub (1:1000 dilution; Millipore, ABS1513), anti-PINK1 (1:1,000; Novus, BC100-494; or 1:1,000; Cell Signaling Technology, clone D8G3), anti-Ub (1:1,000; Ub2, made in-house, (Shiba-Fukushima et al., 2014)), anti-human Parkin (1:1,000; Cell Signaling Technology, clone PRK8), anti-Mfn1 (1:1,000; Abnova, clone 3C9), anti-Tom20 (1:1,000; Santa Cruz Biotechnology, FL-145 or F-10), anti-Tim23 (1:2,000; BD, clone 32/Tim23), anti-LDH (1:500; Santa Cruz Biotechnology, H-160), anti-GFP (1:1,000; MBL, code No. 598), anti-MBP (1:1,000; New England BioLabs, E8030), anti-OPA1 (1:1,000; BD, 612606), anti-TBK1 pS172 (1:1,000; Cell Signaling Technology, clone D52C2), anti-TBK1 (1:1,000; Cell Signaling Technology, clone D1B4), anti-TH (1:1,000; Millipore, clone LNC1), anti-OTC (1:1000; Santa Cruz Biotechnology, clone E-9), anti-Actin (1:10,000; Millipore, MAB1501), and anti-Hsp60 (1:10,000; BD Biosciences, clone 24/Hsp60; 1:1000; Cell Signaling Technology, clone D307). The following antibodies were used for immunocytochemistry: anti-Tom20 (1:1,000; Santa Cruz Biotechnology, FL-145 or F-10), anti-PINK1 (1:100 prepared in Takeda), and anti-TH (1:1,000; Abcam, ab76442).

Val, antimycin, and oligomycin A were purchased from Sigma-Aldrich, Santa Cruz bio, and Cayman Chemical, respectively.

## *In vitro* kinase assay

An *in vitro* kinase assay for PINK1 was performed using maltose-binding protein (MBP) fusion-*T. castaneum* PINK1 (TcPINK1) and bovine ubiquitin (Sigma-Aldrich). MBP-TcPINK1 (500 nM) was preincubated with T0466 in 40 µl of kinase reaction buffer (50 mM Tris-HCl, pH 7.5, 0.1 mM EGTA, 10 mM $MgCl_2$, 2 mM DTT, and 2 mM ATP) for 30 min at 22°C and further incubated with 1 µM of ubiquitin for 90 min at 30°C. For PKA kinase assay, the PKA catalytic subunit (2 units, Sigma-Aldrich, P2645) was preincubated with T0466 for 30 min at 22°C in 40 µl of kinase reaction buffer (50 mM Tris-HCl, pH 7.5, 0.1 mM EGTA, 10 mM $MgCl_2$, 2 mM DTT, and 10 µCi γ-$^{32}$P ATP) and further incubated with 1 µM GST-MIC60 for 90 min at 30°C.

## Thermal shift assay

Recombinant Parkin (0.58 µM, Ubiquigent) in a reaction buffer containing 20 mM HEPES, pH 7.6, 10 mM $MgCl_2$, 2 mM DTT, 1 mM EGTA, SYPRO Orange (1:30 dilution, Thermo Fisher Scientific) with or without cpds was incubated at 22°C for 20 min and transferred into a MicroAmp Optical 384 plate (10 µl/well). Changes in a thermal stability of Parkin due to the addition of cpds was assessed as shifts of fluorescent signals using ABI7900 (Applied Biosystems). Raw data at 25-99°C (at a rate of 1°C/min) were retrieved using Genedata Screener for TSA, and melt curves were generated by plotting the fluorescent signal or the first derivative of the fluorescent signal as a function of temperature.

## Biochemical fractionation of cultured cells

HeLa/GFP-Parkin cells treated with drugs were suspended in mitochondrial isolation buffer (220 mM mannitol, 70 mM sucrose, 20 mM HEPES-KOH pH 7.4, 1 mM EDTA and protease inhibitor cocktail [Roche]), then homogenized by 30 passages using a 26-G needle on ice. Homogenates were centrifuged at 700 *g* for 10 min at 4°C to obtain a post-nuclear supernatant (PNS). The PNS was further centrifuged at 12,000 *g* for 15 min. The supernatant served as a cytosolic fraction. The resultant pellets were washed several times with the mitochondrial isolation buffer and served as a mitochondrial fraction.

## Human iPSCs

Normal iPSC (201B7) lines were differentiated into dopaminergic neurons by our reported protocol (Shiba-Fukushima et al., 2017). Briefly, dissociated neurospheres were allowed to adhere to poly-L-ornithine (Sigma-Aldrich) and laminin (GIBCO)-coated cultured plates or coverslips (Matsunami) and cultured in media hormone mix containing B27 (GIBCO), 10 ng/ml brain-derived neurotrophic factor (BDNF; R&D systems), 10 ng/ml glial cell-derived neurotrophic factor (GDNF; R&D systems), 200 mM ascorbic acid (Sigma-Aldrich), 1 mM dibutyryl-cAMP (Sigma-Aldrich), 1 ng/ml TGF-β (R&D systems) and 10 µM DAPT (Sigma-Aldrich) for 14 days to allow for differentiation into dopaminergic neurons. iCell skeletal myoblasts (SKM-301-020-001-PT) were provided by Cellular Dynamics and cultured, according to the manufacturer's instructions. Cellular and mitochondrial toxicities were estimated using the Mitochondrial ToxGlo Assay kit (Promega) and a multimode plate reader (Mithras$^2$ LB943, Berthold technologies).

## Imaging of cell cultures and western blotting

HeLa and stable cell line imaging was performed using cultures plated on imaging chambers that had been precoated with poly-L-ornithine- and fibronectin (Corning Falcon Chambered Cell Culture Slides, 354104, Thermo Fisher Scientific). For imaging of neuron and skeletal myoblast cultures, cells were plated on poly-L-ornithine- and fibronectin-coated coverslips and stained with antibodies as described (Shiba-Fukushima et al., 2012). The cells were imaged using a laser-scanning microscope system (TCS-SP5, Leica or Zeiss LSM880 with Airyscan). For line profile analysis of human dopaminergic neuron culture, image stacks were acquired at 1 µm intervals using a 40x oil immersion objective with the pinhole diameter set to 1 airy unit using Zeiss LSM880 with Airyscan. Images were reconstructed using a series of stacked images using Zen software (Zeiss) and fluorescence intensity of cross-sections was measured using ImageJ (Fiji) plot-profile tool. Cells were lysed on ice with lysis buffer containing 0.2% NP-40, 50 mM Tris (pH 7.4), 150 mM NaCl and 10% glycerol supplemented

with protease inhibitor (Nacalai) and phosphatase inhibitor (Nacalai) cocktails. Western blotting using cell lysate was performed using ECL prime solution (GE Healthcare) (Shiba-Fukushima et al., 2017). Blot images were obtained using an Image Quant LAS 4000 mini (GE Healthcare).

### Crawling assay

Flies expressing *PINK1 shRNA* in the muscles (*MHC-GAL4, UAS-PINK1 RNAi*) have been reported elsewhere (Yang et al., 2006). Flies expressing *LacZ shRNA* (a gift from Dr. S. Kawabata at Kyusyu University) were used as a control. First instar larvae were raised until the third instar larval stage on 1% agarose plates, where a yeast chunk (600 mg yeast powder kneaded with 1 ml distilled water) containing cpds was mounted. The same amounts of DMSO were used as a cpd solvent in each group. Third instar larvae treated with cpds were placed on the center of a 2% agarose plate (100 mm diameter) and their movement recorded every 10 sec during for 2 min. The movement trace and velocity in the last 60 sec were analyzed by ImageJ (Fiji).

### Mitochondrial morphology in *Drosophila*

For Fig. 4, Fig. S5 and Videos, filets of third instar larvae expressing *MHC-GAL4* driven *mitoGFP* and *PINK1 shRNA* or *LacZ shRNA* were prepared in the HL-3 solution (70 mM NaCl, 5 mM KCl, 20 mM $MgCl_2$, 5 mM trehalose, 115 mM sucrose, 5 mM HEPES, and 10 mM $NaHCO_3$, pH 7.2) and fixed with 4% paraformaldehyde/phosphate buffered saline. Muscle tissues were counterstained with 25 ng/ml TRITC-labeled phalloidin (Sigma-Aldrich) and 1 µg/ml DAPI (Dojindo) at 4°C overnight. For Fig. 5, brain tissues of third instar larvae expressing *TH-GAL4* driven *mitoGFP* and *PINK1 shRNA* or *LacZ shRNA* were isolated in the HL-3 solution and fixed with 4% paraformaldehyde/phosphate buffered saline. Brain tissues were counterstained with anti-TH (in-house, 1:250) (Yang et al., 2006). Image stacks were acquired at 0.35 µm intervals using a 63x oil immersion objective with the pinhole diameter set to 1 airy unit by SP5 (Leica). Images were reconstructed using a series of stacked images with ImageJ Z-projection tool. The volume of mitochondrial aggregates was measured by using IMARIS software (ver. 9.5.0, Bitplane).

### Measurement of mitochondrial ATP and $Ca^{2+}$ dynamics in *Drosophila*

Tissue ATP contents were analyzed using the CellTiter-Glo® Luminescent Cell Viability Assay (Promega). After drug treatment, 100 µl CellTiter-Glo® Reagent was added to *Drosophila* larval homogenates in white 96-well plates and samples were incubated according to the manufacturer's instruction. The effects of bacterial flora in the gut were negligible in this assay, so whole bodies were subjected to ATP measurement. ATP levels were estimated as luminescence intensity measured using a Mithras[2] LB943 plate reader. Luminescence intensities were standardized to the amounts of tissue soluble proteins measured using the Pierce BCA Protein Assay Kit (Thermo Fisher Scientific).

*UAS-mitoGCaMP6* is a construct with the N-terminus of GCaMP6s harbors the mitochondrial targeting sequence of *Drosophila* Hsp60 (CG12101, 1-64 aa). Transgenic flies carrying *UAS-mitoGCaMP6* were generated in the $w^{1118}$ background (BestGene). Filets of third instar larvae expressing *mitoGCaMP6* and *PINK1 shRNA* or *LacZ shRNA* under the control of the *MHC-GAL4* driver were prepared in the HL-3 solution, including 2 mM $Ca^{2+}$, and positioned on a silicone plate using insect pins. Brain tissues were removed and axons of the motor neurons projecting to the abdominal segment three muscles were sucked by a glass electrode. Changes in mitoGCaMP6 fluorescence intensity when electrically stimulated by 2.5 V (500 msec duration) at 20 sec-intervals were recorded using an Eclipse FN1 microscope (Nikon) equipped with an electrical stimulation setup containing a SEN-3401 (Nihon koden) and SS-104J (Nihon koden). The amount of fluorescence change ($\Delta$F/F) was analyzed using ImageJ.

### Quantification of PINK1 transcripts in *Drosophila*

Third-instar larval body-wall muscles were dissected after drug treatment. Total RNA purified with TRIzol (Thermo Fisher Scientific) from three larval pools was subjected to reverse transcription and subsequent quantitative PCR using SuperScript IV VILO and SYBR GreenER (Thermo Fisher Scientific). Quantitative PCR was performed with QuantStudio 7 Flex (Applied Biosystems) using the following primers: dPINK1(ex1)-Fw, 5'-GCGCAGCTATTGTAAACGTGATATACAC;

dPINK1(ex2)-Rv, 5'-TGAGGATGTTGTCGATGAACAATTTGC; RP49 Fw, 5'-CCAAGGACTTCATCCGCCACC; RP49 Rv, 5'-GCGGGTGCGCTTGTTCGATCC.

**Statistical analysis**

Error bars in graphs represent mean ± the standard error of the mean unless otherwise indicated. The exact sample size of each experiment is provided in the relevant figure legends. Two-tailed student's *t*-test or one-way analysis of variance (ANOVA) was used to determine significant differences between two or among multiple groups, respectively, unless otherwise indicated. If a significant result was determined using ANOVA ($p < 0.05$), the mean values of the control and the specific test group were analyzed using a Tukey-Kramer test. Dunnett's test was used to detect significant differences between two specific groups or among multiple groups.

**Supplemental References**

Akabane, S., Uno, M., Tani, N., Shimazaki, S., Ebara, N., Kato, H., Kosako, H., and Oka, T. (2016). PKA Regulates PINK1 Stability and Parkin Recruitment to Damaged Mitochondria through Phosphorylation of MIC60. Molecular cell *62*, 371-384.

Jin, S.M., and Youle, R.J. (2013). The accumulation of misfolded proteins in the mitochondrial matrix is sensed by PINK1 to induce PARK2/Parkin-mediated mitophagy of polarized mitochondria. Autophagy *9*, 1750-1757.

Kane, L.A., Lazarou, M., Fogel, A.I., Li, Y., Yamano, K., Sarraf, S.A., Banerjee, S., and Youle, R.J. (2014). PINK1 phosphorylates ubiquitin to activate Parkin E3 ubiquitin ligase activity. The Journal of cell biology *205*, 143-153.

Shiba-Fukushima, K., Arano, T., Matsumoto, G., Inoshita, T., Yoshida, S., Ishihama, Y., Ryu, K.Y., Nukina, N., Hattori, N., and Imai, Y. (2014). Phosphorylation of mitochondrial polyubiquitin by PINK1 promotes Parkin mitochondrial tethering. PLoS genetics *10*, e1004861.

Shiba-Fukushima, K., Imai, Y., Yoshida, S., Ishihama, Y., Kanao, T., Sato, S., and Hattori, N. (2012). PINK1-mediated phosphorylation of the Parkin ubiquitin-like domain primes mitochondrial translocation of Parkin and regulates mitophagy. Scientific reports *2*, 1002.

Shiba-Fukushima, K., Ishikawa, K.I., Inoshita, T., Izawa, N., Takanashi, M., Sato, S., Onodera, O., Akamatsu, W., Okano, H., Imai, Y.*, et al.* (2017). Evidence that phosphorylated ubiquitin signaling is involved in the etiology of Parkinson's disease. Human molecular genetics *26*, 3172-3185.

Yang, Y., Gehrke, S., Imai, Y., Huang, Z., Ouyang, Y., Wang, J.W., Yang, L., Beal, M.F., Vogel, H., and Lu, B. (2006). Mitochondrial pathology and muscle and dopaminergic neuron degeneration caused by inactivation of Drosophila Pink1 is rescued by Parkin. Proceedings of the National Academy of Sciences of the United States of America *103*, 10793-10798.